of titer and drug susceptibility of HIV-1, respectively. Forty-eight hours after the viral exposure, all the blue cells stained with X-Gal were counted in each well. Viral titer was determined with the MAGI assay as blue cell forming units (BFUs). The activity of test compounds was determined as the concentration that blocked HIV-1 replication by 50% (EC_{50}).

2.4. Viral replication kinetics assay

MT-2 cells (10^5 cells) were infected with each virus preparation (500 BFUs) derived from molecular-constructed clone for 4 h. The infected cells were washed and cultured in a volume of 3 ml. The culture supernatants were harvested on day 4 after infection during the linear replication phase and p24 antigen production was determined (Hachiya et al., 2008). For competitive HIV-1 replication assays (CHRA), the two titrated infectious clones were mixed and added to MT-2 cells as described previously (Nameki et al., 2005). To ensure that the two infectious clones being compared were of approximately equal infectivity, a fixed amount (500 BFUs) of one infectious clone was mixed with three different amounts (250, 500 and 1000 BFUs) of the other infectious clone. On day 1, one-third of the infected MT-2 cells were harvested, and subjected to DNA extraction. The purified DNA was used for nested PCR and then direct sequencing. Every 4–5 days, the viral population change was also determined, and the cell-free supernatant of the virus coculture (1 ml) was transmitted to new uninfected MT-2 cells. The cells harvested at the end of each passage were subjected to direct sequencing, and the viral population change was determined.

2.5. GenBank accession numbers

All sequences of clinical isolates referred in this study are available under GenBank accession nos. AF500084 to AF500093, AJ964904 to AJ964940, AY185366 to AY185492, AY436381 to AY436401, AY523979 to AY523991, AY750998 to AY751078, AY768582 to AY768660, and AY785131 to AY785135.

3. Results

3.1. T-20 susceptibility of HIV-1 clones

V38A, N43D, and a combination of Q40H and L45M conferred strong resistance to T-20 (more than 48-fold) while the Q40H, N43K, and L45M substitutions conferred moderate resistance (5.4–13-fold) in comparison to NL4-3 (wild type, WT) (Table 1). These results are consistent with those of a previous report (Labrosse et al., 2006; Lu et al., 2004; Menzo et al., 2004; Pérez-Alvarez et al., 2006; Wei et al., 2002) and demonstrate that these substitutions act as a primary mutation for T-20 resistance. All synonymous mutations at 39, 41, and 44 conferred little T-20 resistance by themselves and even in combination with other substitutions, including N43D and N43K (Table 1). Since Q39, located adjacent to stem-loop III, has no complementary partner, Q39 was used for further experiments as a control for synonymous mutations. Therefore, the gp41 amino acid sequence solely confers T-20 resistance, while the RNA sequence or the structure itself may not markedly contribute to T-20 resistance.

Although the D36G substitution located in the stem-loop II is observed in the vast majority of HIV-1 strains, only NL4-3 strain contains D36 at this position. The introduction of D36G into NL4-3 based T-20 resistant clones enhanced T-20 susceptibility by approximately 10-fold (Table 1). The D36G partially or completely restored T-20 susceptibility attenuated by N43D or K in NL4-3 viruses, respectively. Therefore, D36 may actually enhance T-20 resistance caused by N43D or N43K in the vast majority of the HIV-1 strains. In fact, D36 is frequently detected in T-20 experienced patients and is associated with T-20 resistance (Cabrera et al., 2006). However, N43K containing variants with D36G background seem to be insufficient for resistance to T-20 (only 4-fold resistance), which is consistent with low frequency of emergence of N43K containing variants in T-20-experienced patients (Lu et al., 2006; Morozov et al., 2007; Si-Mohamed et al., 2007).

3.2. Replication kinetics

In D36 background (pNL4-3 derived virus), replication of HIV-1 with primary mutation(s) was much attenuated (Table 1). It is well consistent with rare frequency of simultaneous introduction of V38A and/or N43D with D36 in vivo (Cabrera et al., 2006). Synonymous substitutions at amino acids, Q41 and L44 were frequently observed in T-20-resistant clinical isolates with N43 substitutions deposited in the GenBank, suggesting that these synonymous mutations may work as secondary mutations. To prove this hypothesis, N43D mutants were generated with synonymous mutations, L44L-CUG: UUG → CUG, Q39Q-CAA: CAG → CAA and Q41Q-CAA: CAG → CAA, designated as HIV-$1_{N43D/L44L-CUG}$, HIV-$1_{Q39Q-CAA/N43D}$ and HIV-$1_{Q41Q-CAA/N43D}$, respectively, and their replication kinetics were determined. The p24 production of all of the mutants remained less than 2% in comparison to that of HIV-1WT (Table 1). Replication kinetics were compared based on CHRA, demonstrating that combination of synonymous and complementary mutations, Q41Q-CAA and L44L-CUG restored replication kinetics impaired by N43D, while that of a simple synonymous mutation (not complementary), Q39Q-CAA, did not (Table 2). However, the D43N (GAU → AAU) substitution, which reverts to WT sequence, was detected in the virus population as early as on day 10 during the CHRA, when HIV-1N43D was used (Fig. 2). N43D (GAU) is the putative target site of apobec3F or 3G deamination that is involved in innate immunity to HIV-1 infection (Bishop et al., 2004; Harris et al., 2003; Liddament et al., 2004; Mangeat et al., 2003; Wiegand et al., 2004; Zhang et al., 2003). The MT-2 cells used in this study express both apobec 3G and 3F as confirmed by reverse transcription 165 coupled PCR (data not shown). Therefore, N43D might be reverted to N43 (identical sequence of HIV-1WT) by the deaminases, thus resulting in the appearance of NL4-3 strains.

Since D36G increases the level of replication by controlling the fusogenic activity (Kinomoto et al., 2005) and stability of RRE structure (Nameki et al., 2005), the generated N43D mutants were combined with D36G (HIV-$1_{D36G/N43D}$, HIV-$1_{D36G/N43D/L44L-CUG}$, HIV-$1_{D36G/Q39Q-CAA/N43D}$ and HIV-$1_{D36G/Q41Q-CAA/N43D}$). These recombinant viruses showed comparable replication kinetics with HIV-1WT or HIV-1_{D36G} (Table 1) and revealed an identical order of replication observed in the N43D containing HIV-1s by the CHRA (Table 2). It is likely that N43D mainly impaired replication kinetics through altered fusion kinetics, since reduced replication kinetics by N43D can be partially restored by introduction of S138A (Cabrera et al., 2006; Marcial et al., 2006; Mink et al., 2005; Xu et al., 2005) and the ΔG value is identical to that of WT (Fig. 1B). It is also possible that nucleotide sequence of N43D-GAT may influence Rev binding to stem III.

In N43K mutants, the synonymous mutation, L44L-CTG, also enhanced the replication kinetics (Table 2). The L44L-CTG enhancement was greater in N43K-AAA mutant. Taken together, synonymous and complementary mutations restore HIV-1 replication impaired by introduced primary mutations, suggesting that these mutations act as secondary mutations.

3.3. Stability of stem-loop III

The structural stability of stem-loop III for N43K with codons AAA or AAG, were both comparable (Fig. 1) when calculated using

Table 1
Drug susceptibility[a] and viral replication[b] of HIV-1 clones with primary mutations or synonymous mutations.

Mutation(s)	EC_{50} [c] (μM)		p24(%)
	ddC	T-20	
WT[d]	0.51 ± 0.089	0.021 ± 0.0093	100
D36G	0.66 ± 0.22 (1.3)[e]	0.0026 ± 0.0012 (0.1)	95 ± 15
Primary mutations			
V38A	0.65 ± 0.12 (1.3)	>1.0 (>48)	3.3 ± 1.7
Q40H	0.47 ± 0.11 (0.9)	0.21 ± 0.087 (10)	31 ± 11
N43D	0.48 ± 0.13 (0.9)	>1.0 (>48)	<2
$N43K_{AAA}$	0.22 ± 0.005 (0.4)	0.28 ± 0.024 (13)	21 ± 11
$N43K_{AAG}$	0.32 ± 0.009 (0.6)	0.11 ± 0.019 (5.4)	30 ± 16
L45M	0.68 ± 0.12 (1.3)	0.27 ± 0.11 (13)	5.4 ± 0.8
Q40H/L45M	0.37 ± 0.2 (0.7)	>1.0 (>48)	7.7 ± 3.7
Synonymous mutations			
$Q_{CAG}39Q_{CAA}$	0.62 ± 0.077 (1.2)	0.015 ± 0.006 (0.7)	115 ± 16
$Q_{CAG}41Q_{CAA}$	0.58 ± 0.13 (1.1)	0.054 ± 0.011 (2.6)	192 ± 53
$L_{UUG}44L_{CUG}$	0.62 ± 0.089 (1.2)	0.030 ± 0.018 (1.5)	191 ± 34
$L_{UUG}44L_{UUA}$	0.64 ± 0.18 (1.3)	0.014 ± 0.0026 (0.7)	5.9 ± 1.7
N43D series			
N43D[f]	0.48 ± 0.13 (0.9)	>1.0 (>48)	<2[g]
$N43D/L44L_{CUG}$	0.35 ± 0.050 (0.7)	>1.0 (>48)	<2
$Q39Q_{CAA}/N43D$	0.34 ± 0.17 (0.7)	>1.0 (>48)	<2
$Q41Q_{CAA}/N43D$	0.62 ± 0.097 (1.2)	>1.0 (>48)	<2
D36G/N43D	0.56 ± 0.18 (1.1)	0.13 ± 0.056 (6.1)	81 ± 10
$D36G/N43D/L44L_{CUG}$	0.63 ± 0.19 (1.2)	0.10 ± 0.045 (4.9)	103 ± 34
$D36G/Q39Q_{CAA}/N43D$	0.76 ± 0.12 (1.5)	0.14 ± 0.057 (6.8)	59 ± 23
$D36G/Q41Q_{CAA}/N43D$	0.74 ± 0.14 (1.5)	0.14 ± 0.066 (6.8)	67 ± 16
N43K series			
$N43K_{AAA}$ [f]	0.22 ± 0.005 (0.4)	0.28 ± 0.024 (13)	21 ± 11
$N43K_{AAG}$ [f]	0.32 ± 0.009 (0.6)	0.28 ± 0.077 (13)	30 ± 16
$N43K_{AAA}/L44L_{CUG}$	0.64 ± 0.087 (1.3)	0.22 ± 0.082 (11)	76 ± 18
$N43K_{AAG}/L44L_{CUG}$	0.59 ± 0.10 (1.2)	0.20 ± 0.067 (10)	37 ± 15
$D36G/N43K_{AAA}$	0.61 ± 0.086 (1.2)	0.0069 ± 0.0004 (0.3)	26 ± 18
$D36G/N43K_{AAG}$	0.60 ± 0.078 (1.2)	0.0087 ± 0.0008 (0.4)	27 ± 12
$D36G/N43K_{AAA}/L44_{CUG}$	0.28 ± 0.14 (0.6)	0.0057 ± 0.0016 (0.3)	96 ± 19
$D36G/N43K_{AAG}/L44L_{CUG}$	0.69 ± 0.14 (1.4)	0.0069 ± 0.0003 (0.3)	53 ± 8.1

[a] Antiviral activity was determined by the MAGI assay. The data shown are mean values and standard deviations obtained from the results of at least three independent experiments.

[b] Viral replication was determined by p24 ELISA. The data shown are mean values and standard deviations obtained from the results of at least three independent experiments. Absolute p24 value for $HIV\text{-}1_{WT}$ was 1.8 ± 0.2 ng/ml.

[c] 50% effective concentration was determined with the MAGI assay (Nameki et al., 2005).

[d] $HIV\text{-}1_{NL4\text{-}3}$ was used as a wild type virus.

[e] Fold change in EC_{50} of the gp41 recombinant molecular clone compared with that of $HIV\text{-}1_{WT}$.

[f] Also described in the *primary mutations* section of Table 1.

[g] Only insufficient replication of $HIV\text{-}1_{N43D}$ in MT-2 cells was observed. However, we could determine initial titer of the $HIV\text{-}1_{N43D}$ obtained from freshly transfected 293T cells in the MAGI cells, since the MAGI assay only detects first round of viral infection up to Tat expression. Therefore, it may be ideal for determination of accurate inhibitory effect compared to other assays that allow multiple replications.

the MFold program version 3.2 (http://frontend.bioinfo.rpi.edu/applications/mfold/) (Mathews et al., 1999; Zuker, 2003). The replication kinetics of HIV-1N43K-AAA and HIV-1N43K-AAG were comparable, in combination of L44L-CTG, however, that of HIV-1N43K-AAA was greater by the CHRA. It is possible that the nucleotide sequence itself may affect binding affinity of Rev to the RRE, although detailed mechanism of the difference between N43K-AAA and -AAG remains to be elucidated. Introduction of D36G to N43K-containing clones did not improve the replication kinetics of N43K-containing clones but restored their susceptibilities to T-20 (Table 1). These results indicate that synonymous mutations thus maintain HIV-1 replication.

A combination of primary mutations, namely Q40H and L45M (both ΔG values are 0.1 but in combination that is −4.5), which are complementarily located and stabilize stem III structure (Fig. 1B) and observed in vivo (Cabrera et al., 2006; Marcial et al., 2006; Mink et al., 2005; Xu et al., 2005), may alter the replication kinetics at either the nucleotide or amino acid level. Recent studies also highlight strong co-presence of Q40H and L45M in clinical isolates treated with T-20 (Svicher et al., 2008). These results sug-

Table 2
Effect of synonymous mutations on replication of HIV-1.

Mutation background	Order of replication
N43D	$HIV\text{-}1_{N43D/L44L\text{-}CUG} = HIV\text{-}1_{Q41Q\text{-}CAA/N43D} > HIV\text{-}1_{N43D} = HIV\text{-}1_{Q39Q\text{-}CAA/N43D}$
D36G/N43D	$HIV\text{-}1_{D36G/N43D/L44L\text{-}CUG} = HIV\text{-}1_{D36G/Q41Q\text{-}CAA/N43D} > HIV\text{-}1_{D36G/N43D} > HIV\text{-}1_{D36G/Q39Q\text{-}CAA/N43D}$
N43K	$HIV\text{-}1_{N43K\text{-}AAA/L44L\text{-}CUG} > HIV\text{-}1_{N43K\text{-}AAG/L44L\text{-}CUG} > HIV\text{-}1_{N43K\text{-}AAA} = HIV\text{-}1_{N43K\text{-}AAG}$
Synonymous mutations	$HIV\text{-}1_{L44L\text{-}CUG} = HIV\text{-}1_{Q41Q\text{-}CAA} > HIV\text{-}1_{WT} = HIV\text{-}1_{Q39Q\text{-}CAA}$

Competition of HIV-1 replication assay (CHRA) was performed in MT-2 cells. At least two independent CHRAs were performed.

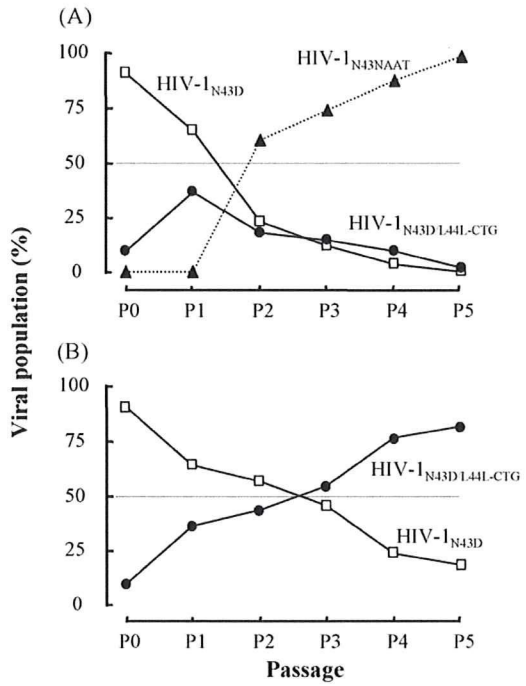

Fig. 2. Emergence of HIV-$1_{N43N\text{-}AAT}$ (HIV-1_{WT}) during CHRA for HIV-1_{N43D} and HIV-$1_{N43D/L44L\text{-}CTG}$ are shown. Open square, closed circle, and closed triangle represent HIV-1_{N43D}, HIV-$1_{N43D/L44L\text{-}CTG}$, and HIV-$1_{N43N\text{-}AAT}$, respectively. Absolute viral populations of each HIV-1s (A) and relative viral populations of HIV-1_{N43D} and HIV-$1_{N43D/L44L\text{-}CTG}$ (B) were shown.

gest that introduction of the primary mutations in the nucleotide level are affected by the RRE stability, indicating that amino acid and nucleotide substitutions in the gp41 and the RRE, respectively, co-operatively play a role.

3.4. *Effect of synonymous mutations*

As expected, the synonymous mutations (Q39Q-CAA, Q41Q-CAA, and L44L-CUG) solely affect viral replication but not T-20 susceptibility (0.7–2.6-fold in Table 1). They displayed an order of replication of HIV-1L44L-CUG = HIV-1Q41Q-CAA > HIV-1WT = HIV-1Q39Q-CAA, also demonstrating that only synonymous and complementary mutations, Q41Q-CAA and L44L-CTG, enhance replication kinetics. Finally, HIV-1L44L-UUA that is not detected in vivo was constructed and its replication kinetics was examined. As shown in Fig. 1, the third nucleotide for L44 raises the ΔG value, thus indicating that structure of the stem-loop III is unstable. The variants displayed impaired replication kinetics (Table 1). These results indicate that, in addition to the influence on gp41 function by amino acid substitutions, the structural stability of stem-loop III is one of the major determinants of the replication kinetics of mutated clones.

4. Discussion

This study demonstrated that synonymous mutations in the stem-loop III of RRE play an important role in the improvement of HIV-1 replication without affecting T-20 susceptibility. The structural stability of stem-loop III defined by ΔG value was strongly correlated with the replication kinetics ($R^2 = 0.76$, Fig. 1C), while the susceptibility, based on the EC_{50} value, was less ($R^2 < 0.3$ excluding clones that showed over 48-fold resistance, data not shown). Although it is likely that the nucleotide sequence of stem-loop III as well as the structural stability may also influence the RRE functions, including Rev binding, the current results indicate that the structural stability of RRE as well as gp41 amino acid substitutions seem to be a determinant for replication kinetics. At present, however, it is impossible to conclude that the pre-existence of such synonymous mutations in the RRE predicts on how T-20 resistance mutations are acquired.

Armand-Ugón et al initially isolated and reported resistance to C34 in vitro (Armand-Ugón et al., 2003), although we previously demonstrated that some of mutations for C34 resistance are involved in the RRE function as described (Nameki et al., 2005). The variants contained L33S or V38E mutations in the gp41 and both showed strong (more than 500-fold resistance) C34 resistance (Armand-Ugón et al., 2003). These mutations in the nucleotide level are also located in RRE (Fig. 1A); the nucleotide substitutions for L33S and V38E are located in the loop of stem IIB and the middle of stem IIC, respectively. Interestingly, V38E emerged in the HxB2-derived strain containing D36G polymorphism that stabilizes stem IIB structure, while L33S, which might have little effect on stem IIC stability due to its location, was observed in the NL4-3-derived resistant strain. These results also suggest that introduction of some mutations in the gp41 is restricted by RRE function. Armand-Ugón et al. (2003) failed to identify the secondary mutations for L33S or V38E. It is likely that the effect on RRE function may be tolerable for viral replication. Alternatively, relative short induction periods (maximum 17 passages) might also influence efficient introduction of the secondary mutations.

Functional analysis for Rev, RRE, and/or both seems to be important to reveal a detailed effect on viral replication. In this regard, we have previously demonstrated that effect of mutations for C34 resistance located in stem-loop II on binding of Rev to RRE was not apparent (less than 10% in the gel shift assay (Nameki et al., 2005)). It is possible that other factors including nuclear export and host factors, which may be influenced by the mutations, are involved in viral replication through interaction of Rev/RRE in HIV infected cells. Therefore, in the present study, we constructed an artificial mutant L44-TTA, which destabilizes or disrupts the stem III structure, and examined the effect on viral replication (Table 1). Replication of L44-TTA containing mutant showed much reduced replication kinetics even without gp41 amino acid substitutions, again indicating that stem III also plays an important role in viral replication.

So far, no information concerning Rev and Tat nucleotide substitutions is available in T-20 experienced patients. It is possible that the altered function of RRE may induce Rev mutation(s). In this regard, the entire sequence of Rev coding region of a C34 resistant variant was determined, however, no mutations were observed (Nameki et al., 2005). Most of the coding region of Rev also encodes Tat and gp41, thus indicating that Rev mutation(s) would alter these functions. This suggests that, even for single amino acid substitution, the genetic barrier for T-20 resistance seems to be relatively high when synonymous mutations are required to be introduced with the primary mutations and further fusion inhibitors that target the N-helical region thus appear to be promising.

In conclusion, this study provides valuable insight into the functional importance of RRE in HIV-1 with T-20 resistance for the replication kinetics. To reveal the function of gp41, experiments with artificial amino acid substitutions, *e.g.*, alanine scanning, which can be used to rapidly identify residues important for protein function by alanine substitution, should be carefully conducted. Further studies will reveal the functional significance of the RNA and protein function in this region.

Acknowledgements

HeLa-CD4-LTR-β-gal cells were kindly provided by Dr. M. Emerman through the AIDS Research and Reference Reagent Program,

Division of AIDS, National Institute of Allergy and Infectious Disease (Bethesda, MD). M.U., K.S., Y. Sakurai., and K.K. were supported by the 21st Century COE program of the Ministry of Education, Culture, Sports, Science, and Technology. This work was supported by grants for the promotion of AIDS Research from the Ministry of Health, Labor, and Welfare and Research for Health Sciences Focusing on Drug Innovation from The Japan Health Sciences Foundation (E.N.K., S.O., N.F., and M.M.).

References

Armand-Ugón, M., Gutiérrez, A., Clotet, B., Esté, J.A., 2003. HIV-1 resistance to the gp41-dependent fusion inhibitor C-34. Antiviral Res. 59, 137–142.

Bishop, K.N., Holmes, R.K., Sheehy, A.M., Davidson, N.O., Cho, S.J., Malim, M.H., 2004. Cytidine deamination of retroviral DNA by diverse APOBEC proteins. Curr. Biol. 14, 1392–1396.

Cabrera, C., Marfil, S., García, E., Martinez-Picado, J., Bonjoch, A., Bofill, M., Moreno, S., Ribera, E., Domingo, P., Clotet, B., Ruiz, L., 2006. Genetic evolution of gp41 reveals a highly exclusive relationship between codons 36, 38 and 43 in gp41 under long-term enfuvirtide-containing salvage regimen. AIDS 20, 2075–2080.

Fikkert, V., Cherepanov, P., Van Laethem, K., Hantson, A., Van Remoortel, B., Pannecouque, C., De Clercq, E., Debyser, Z., Vandamme, A.M., Witvrouw, M., 2002. env chimeric virus technology for evaluating human immunodeficiency virus susceptibility to entry inhibitors. Antimicrob. Agents Chemother. 46, 3954–3962.

Fung, H.B., Guo, Y., 2004. Enfuvirtide: a fusion inhibitor for the treatment of HIV infection. Clin. Ther. 26, 352–378.

Hachiya, A., Kodama, E.N., Sarafianos, S.G., Schuckmann, M.M., Sakagami, Y., Matsuoka, M., Takiguchi, M., Gatanaga, H., Oka, S., 2008. Amino acid mutation N348I in the connection subdomain of human immunodeficiency virus type 1 reverse transcriptase confers multiclass resistance to nucleoside and nonnucleoside reverse transcriptase inhibitors. J. Virol. 82, 3261–3270.

Harris, R.S., Bishop, K.N., Sheehy, A.M., Craig, H.M., Petersen-Mahrt, S.K., Watt, I.N., Neuberger, M.S., Malim, M.H., 2003. DNA deamination mediates innate immunity to retroviral infection. Cell 113, 803–809.

Kimpton, J., Emerman, M., 1992. Detection of replication-competent and pseudotyped human immunodeficiency virus with a sensitive cell line on the basis of activation of an integrated beta-galactosidase gene. J. Virol. 66, 2232–2239.

Kinomoto, M., Yokoyama, M., Sato, H., Kojima, A., Kurata, T., Ikuta, K., Sata, T., Tokunaga, K., 2005. Amino acid 36 in the human immunodeficiency virus type 1 gp41 ectodomain controls fusogenic activity: implications for the molecular mechanism of viral escape from a fusion inhibitor. J. Virol. 79, 5996–6004.

Kodama, E.I., Kohgo, S., Kitano, K., Machida, H., Gatanaga, H., Shigeta, S., Matsuoka, M., Ohrui, H., Mitsuya, H., 2001. 4′-Ethynyl nucleoside analogs: potent inhibitors of multidrug-resistant human immunodeficiency virus variants in vitro. Antimicrob. Agents Chemother. 45, 1539–1546.

Labrosse, B., Morand-Joubert, L., Goubard, A., Rochas, S., Labernardiére, J.L., Pacanowski, J., Meynard, J.L., Hance, A.J., Clavel, F., Mammano, F., 2006. Role of the envelope genetic context in the development of enfuvirtide resistance in human immunodeficiency virus type 1-infected patients. J. Virol. 80, 8807–8819.

Lalezari, J.P., Henry, K., O'Hearn, M., Montaner, J.S., Piliero, P.J., Trottier, B., Walmsley, S., Cohen, C., Kuritzkes, D.R., Eron Jr., J.J., Chung, J., DeMasi, R., Donatacci, L., Drobnes, C., Delehanty, J., Salgo, M., 2003. Enfuvirtide, an HIV-1 fusion inhibitor, for drug-resistant HIV infection in North and South America. N. Engl. J. Med. 348, 2175–2185.

Lazzarin, A., Clotet, B., Cooper, D., Reynes, J., Arasteh, K., Nelson, M., Katlama, C., Stellbrink, H.J., Delfraissy, J.F., Lange, J., Huson, L., DeMasi, R., Wat, C., Delehanty, J., Drobnes, C., Salgo, M., 2003. Efficacy of enfuvirtide in patients infected with drug-resistant HIV-1 in Europe and Australia. N. Engl. J. Med. 348, 2186–2195.

Liddament, M.T., Brown, W.L., Schumacher, A.J., Harris, R.S., 2004. APOBEC3F properties and hypermutation preferences indicate activity against HIV-1 in vivo. Curr. Biol. 14, 1385–1391.

Lu, J., Deeks, S.G., Hoh, R., Beatty, G., Kuritzkes, B.A., Martin, J.N., Kuritzkes, D.R., 2006. Rapid emergence of enfuvirtide resistance in HIV-1-infected patients: results of a clonal analysis. J. Acquir. Immune Defic. Syndr. 43, 60–64.

Lu, J., Sista, P., Giguel, F., Greenberg, M., Kuritzkes, D.R., 2004. Relative replicative fitness of human immunodeficiency virus type 1 mutants resistant to enfuvirtide (T-20). J. Virol. 78, 4628–4637.

Maeda, Y., Venzon, D.J., Mitsuya, H., 1998. Altered drug sensitivity, fitness, and evolution of human immunodeficiency virus type 1 with pol gene mutations conferring multi-dideoxynucleoside resistance. J. Infect. Dis. 177, 1207–1213.

Manfredi, R., Sabbatani, S., 2006. A novel antiretroviral class (fusion inhibitors) in the management of HIV infection. Present features and future perspectives of enfuvirtide (T-20). Curr. Med. Chem. 13, 2369–2384.

Mangeat, B., Turelli, P., Caron, G., Friedli, M., Perrin, L., Trono, D., 2003. Broad antiretroviral defence by human APOBEC3G through lethal editing of nascent reverse transcripts. Nature 424, 99–103.

Marcelin, A.G., Reynes, J., Yerly, S., Ktorza, N., Segondy, M., Piot, J.C., Delfraissy, J.F., Kaiser, L., Perrin, L., Katlama, C., Calvez, V., 2004. Characterization of genotypic determinants in HR-1 and HR-2 gp41 domains in individuals with persistent HIV viraemia under T-20. AIDS 18, 1340–1342.

Marcial, M., Lu, J., Deeks, S.G., Ziermann, R., Kuritzkes, D.R., 2006. Performance of human immunodeficiency virus type 1 gp41 assays for detecting enfuvirtide (T-20) resistance mutations. J. Clin. Microbiol. 44, 3384–3387.

Mathews, D.H., Sabina, J., Zuker, M., Turner, D.H., 1999. Expanded sequence dependence of thermodynamic parameters improves prediction of RNA secondary structure. J. Mol. Biol. 288, 911–940.

Menzo, S., Castagna, A., Monachetti, A., Hasson, H., Danise, A., Carini, E., Bagnarelli, P., Lazzarin, A., Clementi, M., 2004. Genotype and phenotype patterns of human immunodeficiency virus type 1 resistance to enfuvirtide during long-term treatment. Antimicrob. Agents Chemother. 48, 3253–3259.

Mink, M., Mosier, S.M., Janumpalli, S., Davison, D., Jin, L., Melby, T., Sista, P., Erickson, J., Lambert, D., Stanfield-Oakley, S.A., Salgo, M., Cammack, N., Matthews, T., Greenberg, M.L., 2005. Impact of human immunodeficiency virus type 1 gp41 amino acid substitutions selected during enfuvirtide treatment on gp41 binding and antiviral potency of enfuvirtide in vitro. J. Virol. 79, 12447–12454.

Morozov, V.A., Morozov, A.V., Schürmann, D., Jessen, H., Kücherer, C., 2007. Transmembrane protein polymorphisms and resistance to T-20 (Enfuvirtide, Fuzeon) in HIV-1 infected therapy-naive seroconverters and AIDS patients under HAART-T-20 therapy. Virus Genes 35, 167–174.

Nameki, D., Kodama, E., Ikeuchi, M., Mabuchi, N., Otaka, A., Tamamura, H., Ohno, M., Fujii, N., Matsuoka, M., 2005. Mutations conferring resistance to human immunodeficiency virus type 1 fusion inhibitors are restricted by gp41 and Rev-responsive element functions. J. Virol. 79, 764–770.

Olsen, H.S., Nelbock, P., Cochrane, A.W., Rosen, C.A., 1990. Secondary structure is the major determinant for interaction of HIV rev protein with RNA. Science 247, 845–848.

Otaka, A., Nakamura, M., Nameki, D., Kodama, E., Uchiyama, S., Nakamura, S., Nakano, H., Tamamura, H., Kobayashi, Y., Matsuoka, M., Fujii, N., 2002. Remodeling of gp41-C34 peptide leads to highly effective inhibitors of the fusion of HIV-1 with target cells. Angew. Chem. Int. Ed. Engl. 41, 2937–2940.

Pérez-Alvarez, L., Carmona, R., Ocampo, A., Asorey, A., Miralles, C., Pérez de Castro, S., Pinilla, M., Contreras, G., Taboada, J.A., Nájera, R., 2006. Long-term monitoring of genotypic and phenotypic resistance to T20 in treated patients infected with HIV-1. J. Med. Virol. 78, 141–147.

Poveda, E., Rodés, B., Toro, C., Martín-Carbonero, L., Gonzalez-Lahoz, J., Soriano, V., 2002. Evolution of the gp41 env region in HIV-infected patients receiving T-20, a fusion inhibitor. AIDS 16, 1959–1961.

Si-Mohamed, A., Piketty, C., Tisserand, P., LeGoff, J., Weiss, L., Charpentier, C., Kazatchkine, M.D., Bélec, L., 2007. Increased polymorphism in the HR-1 gp41 env gene encoding the enfuvirtide (T-20) target in HIV-1 variants harboring multiple antiretroviral drug resistance mutations in the pol gene. J. Acquir. Immune Defic. Syndr. 44, 1–5.

Sista, P.R., Melby, T., Davison, D., Jin, L., Mosier, S., Mink, M., Nelson, E.L., DeMasi, R., Cammack, N., Salgo, M.P., Matthews, T.J., Greenberg, M.L., 2004. Characterization of determinants of genotypic and phenotypic resistance to enfuvirtide in baseline and on-treatment HIV-1 isolates. AIDS 18, 1787–1794.

Su, C., Melby, T., DeMasi, R., Ravindran, P., Heilek-Snyder, G., 2006. Genotypic changes in human immunodeficiency virus type 1 envelope glycoproteins on treatment with the fusion inhibitor enfuvirtide and their influence on changes in drug susceptibility in vitro. J. Clin. Virol. 36, 249–257.

Svicher, V., Aquaro, S., D'Arrigo, R., Artese, A., Dimonte, S., Alcaro, S., Santoro, M.M., Di Perri, G., Caputo, S.L., Bellagamba, R., Zaccarelli, M., Visco-Comandini, U., Antinori, A., Narciso, P., Ceccherini-Silberstein, F., Perno, C.F., 2008. Specific enfuvirtide-associated mutational pathways in HIV-1 gp41 are significantly correlated with an increase in CD4(+) cell count, despite virological failure. J. Infect. Dis. 197, 1408–1418.

Wei, X., Decker, J.M., Liu, H., Zhang, Z., Arani, R.B., Kilby, J.M., Saag, M.S., Wu, X., Shaw, G.M., Kappes, J.C., 2002. Emergence of resistant human immunodeficiency virus type 1 in patients receiving fusion inhibitor (T-20) monotherapy. Antimicrob. Agents Chemother. 46, 1896–1905.

Wiegand, H.L., Doehle, B.P., Bogerd, H.P., Cullen, B.R., 2004. A second human antiretroviral factor, APOBEC3F, is suppressed by the HIV-1 and HIV-2 Vif proteins. EMBO J. 23, 2451–2458.

Xu, L., Pozniak, A., Wildfire, A., Stanfield-Oakley, S.A., Mosier, S.M., Ratcliffe, D., Workman, J., Joall, A., Myers, R., Smit, E., Cane, P.A., Greenberg, M.L., Pillay, D., 2005. Emergence and evolution of enfuvirtide resistance following long-term therapy involves heptad repeat 2 mutations within gp41. Antimicrob. Agents Chemother. 49, 1113–1119.

Zapp, M.L., Green, M.R., 1989. Sequence-specific RNA binding by the HIV-1 Rev protein. Nature 342, 714–716.

Zhang, H., Yang, B., Pomerantz, R.J., Zhang, C., Arunachalam, S.C., Gao, L., 2003. The cytidine deaminase CEM15 induces hypermutation in newly synthesized HIV-1 DNA. Nature 424, 94–98.

Zuker, M., 2003. Mfold web server for nucleic acid folding and hybridization prediction. Nucleic Acids Res. 31, 3406–3415.

Peptide bond mimicry by (*E*)-alkene and (*Z*)-fluoroalkene peptide isosteres: synthesis and bioevaluation of α-helical anti-HIV peptide analogues†

Shinya Oishi,*[a] Hirotaka Kamitani,[a] Yasuyo Kodera,[a] Kentaro Watanabe,[a] Kazuya Kobayashi,[a] Tetsuo Narumi,[a] Kenji Tomita,[a] Hiroaki Ohno,[a] Takeshi Naito,[b] Eiichi Kodama,[b] Masao Matsuoka[b] and Nobutaka Fujii*[a]

Received 22nd April 2009, Accepted 30th April 2009
First published as an Advance Article on the web 4th June 2009
DOI: 10.1039/b907983a

The α-helix structures of the anti-HIV fusion inhibitory peptides are stabilized by the amino acid sequence and by intrachain hydrogen bonds. The study of peptide analogues using (*E*)-alkene and (*Z*)-fluoroalkene dipeptide isosteres demonstrated the substantial, yet position-dependent, contribution of hydrogen bonds to the α-helix stability and anti-HIV bioactivity.

Introduction

The α-helix represents one of the largest classes of secondary structure elements found in protein and peptide structures.[1] The cylindrical structures are stabilized by intrachain hydrogen bond (H-bond) networks which are formed between the C=O of residue *i* and the amide N–H of the *i*+4 residue to generate 13-membered pseudocyclic structures. The functional and/or interactive surface(s) of the α-helix are revealed by the arrangement of the distribution residues in the linear sequence upon folding.

In order to stabilize the α-helix structure of bioactive peptides, there are two possible approaches: (1) bridging side-chains by covalent or non-covalent bond(s) or (2) mimicking intrachain H-bond(s).[2] Recently, we reported a novel design concept of fusion inhibitory peptides active against HIV-1 by utilizing an X-EE-XX-KK motif (X: original residue; E: glutamic acid; K: lysine).[3,4] This motif contributes to the stabilization of the bioactive α-helix conformation by forming two potential salt bridges between Glu and Lys side-chains without altering the location of residues that form the interactive surface with the viral protein gp41.[4c] The peptides, named SC35EK and T-20EK, exhibit highly potent anti-HIV activity by inhibition of the rearrangement of HIV-1 gp41 that facilitates fusion between the host cellular and viral membranes. In addition, a structure–activity relationship study identified a novel amphiphilic peptide, SC29EK, with a minimal sequence for anti-HIV activity.[5] In light of its high potency of SC29EK, it was of interest to estimate the effect of intrachain H-bond(s) on α-helix stabilization in the presence of the X-EE-XX-KK motifs. Accordingly, efforts herein have been undertaken to comparatively evaluate the anti-HIV activity and biophysical properties of SC29EK analogues containing peptide bond mimetics.

(*E*)-Alkene dipeptide isostere (EADI) **1** and (*Z*)-fluoroalkene dipeptide isostere (FADI) **2** of Lys-Lys were chosen as planar peptide bond surrogates for positional scanning of each Lys-Lys dipeptide in four repeat motifs (Fig. 1).[6] Two potential H-bonds may be missing when replacing the peptide bond in Lys-Lys with the olefin congeners: (1) between the C=O of the first Lys (*i*) and the N–H of the downward Glu (*i*+4), (2) between the N–H of the second Lys (*i*+1) and the C=O of the upward Glu (*i*−3) (Fig. 1). In the case of FADI substitution, the presence of the first H-bond was expected, because of the potential ability of a fluorine atom to act as a H-bond acceptor.[7]

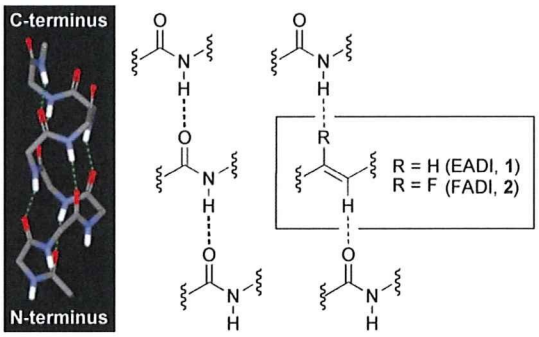

Fig. 1 Structures of (*E*)-alkene and (*Z*)-fluoroalkene dipeptide isosteres and the potential mimicry of H-bonds stabilizing the α-helix structure.

Results and discussion

Lys-Lys EADI[8] and FADI[9] were prepared by the established procedures shown in Schemes 1 and 2, respectively. Briefly, allyl alcohol **3**[10] derived from a protected amino acid was converted into Ns-amide **4**. Aziridination of **4** by the Mitsunobu reaction followed by C-1 elongation afforded the β-aziridinyl-α,β-unsaturated ester **6**. Organocopper-mediated alkylation of **6** provided an α-alkyl adduct **7** regio- and stereoselectively. Subsequent functional group manipulations generated the expected Fmoc-protected EADI **10**.

FADI synthesis began with mono-TBS-protected 1,5-pentanediol **11**. Rh-catalyzed Reformatsky–Honda reaction[11] of the corresponding aldehyde gave α,α-difluoro-β-amino ester **12**. The simultaneous hydrogenolysis and Boc protection followed by C-2 elongation using the Horner–Wadsworth–Emmons reaction produced a key γ,γ-difluoro-α,β-enoyl sultam **14**. One-pot reduction/asymmetric alkylation *via* transmetalation with allyl bromide formed the FADI scaffold **15**. Selective

[a]*Graduate School of Pharmaceutical Sciences, Kyoto University, Sakyo-ku, Kyoto, 606-8501, Japan. E-mail: soishi@pharm.kyoto-u.ac.jp, nfujii@pharm.kyoto-u.ac.jp; Fax: +81-75-753-4570; Tel: +81-75-753-4551*
[b]*Laboratory of Virus Control, Institute for Virus Research, Kyoto University, Sakyo-ku, Kyoto, 606-8507, Japan*

† Electronic supplementary information (ESI) available: Additional experimental procedures, NMR spectra and HPLC charts. See DOI: 10.1039/b907983a

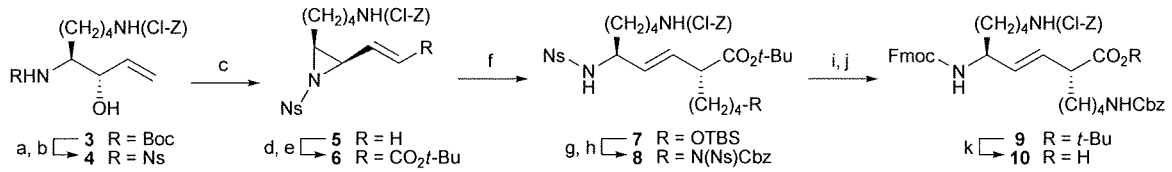

Scheme 1 Synthesis of the Lys-Lys-type alkene dipeptide isostere. *Reagents and conditions*: (a) 4 N HCl/dioxane; (b) NsCl, 2,4,6-collidine, $CHCl_3$, 65% (2 steps); (c) DIAD, PPh_3, THF/toluene, 0 °C, 84%; (d) O_3, AcOEt, −78 °C, then Me_2S; (e) $(EtO)_2P(O)CH_2CO_2t$-Bu, LiCl, DIEA, CH_3CN, 0 °C, 46% (2 steps); (f) $TBSO(CH_2)_4I$, *t*-BuLi, CuCN, LiCl, *n*-pentane/Et_2O/THF, −78 °C, 60%; (g) H_2SiF_6 aq., CH_3CN/CH_3OH, 0 °C; (h) CbzNHNs, PPh_3, DIAD, THF/toluene, 81% (2 steps); (i) PhSH, K_2CO_3, DMF; (j) Fmoc-OSu, Et_3N, DMF, 84% (2 steps); (k) 4 N HCl/dioxane, 96%.

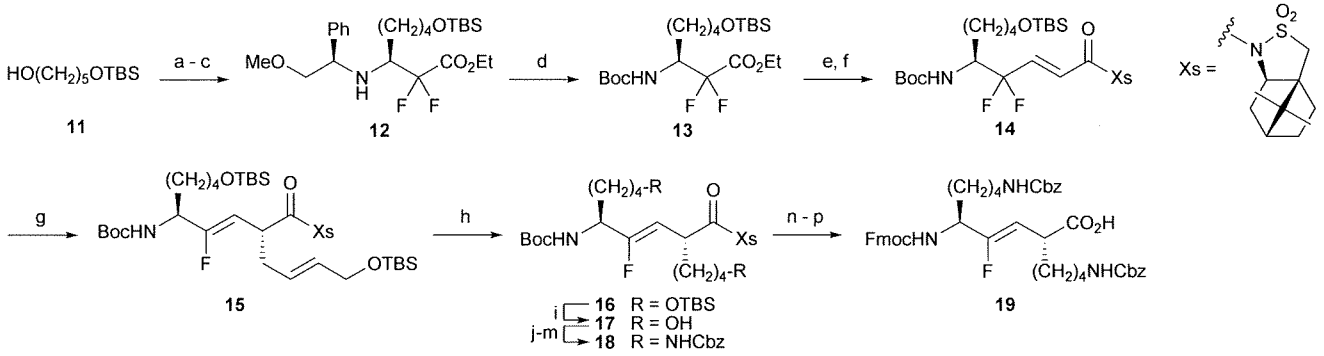

Scheme 2 Synthesis of the Lys-Lys-type fluoroalkene dipeptide isostere. *Reagents and conditions*: (a) DMSO, $(COCl)_2$, Et_3N, CH_2Cl_2, −78 °C; (b) (*R*)-2-methoxy-1-phenylethylamine, 3 Å MS, THF, 0 °C; (c) $BrCF_2CO_2Et$, $RhCl(PPh_3)_3$, Et_2Zn, 0 °C, 43% (3 steps); (d) $Pd(OH)_2$, H_2, Boc_2O, EtOH, 87%; (e) DIBAL-H, CH_2Cl_2/toluene −78 °C; (f) $(EtO)_2P(O)CH_2COXs$, LiCl, DIEA, CH_3CN, 0 °C, 87% (2 steps); (g) $Me_2CuLi{\cdot}LiI$, THF/Et_2O, −78 °C, then HMPA, then Ph_3SnCl, −78 °C to −40 °C, then $BrCH_2$–(*E*)-CH=CH–CH_2OTBS, −40 °C, 78%; (h) 4.5% Pd/C(en), EtOH, H_2; (i) aq. H_2SiF_6, CH_3CN/CH_3OH, 78% (2 steps); (j) TsCl, Et_3N, CH_2Cl_2; (k) NaN_3, DMF; (l) PPh_3, THF/H_2O; (m) Cbz-OSu, Et_3N, DMF, 65% (4 steps); (n) 1 N LiOH, 50% H_2O_2, THF/H_2O; (o) TFA, CH_2Cl_2; (p) Fmoc-OSu, Et_3N, MeCN/DMF/H_2O, 64% (3 steps).

hydrogenation in the presence of Pd/C(en)[12] and step-wise modifications afforded the Fmoc-protected FADI **19**. The resulting isosteres **10** and **19** were incorporated into the KK dipeptide of SC29EK sequence by standard Fmoc-based solid-phase peptide synthesis.

Anti-HIV activities of the isostere-containing peptides **20E–23E** and **20F–23F** were examined using the MAGI assay (Table 1). Substitutions of the first and second N-terminal Lys-Lys dipeptides with EADI (**20E** and **21E**) resulted in the loss of the anti-HIV activity (EC_{50} >10 μM). In contrast, the FADI congeners exhibited weak or moderate anti-HIV activities (**20F**: EC_{50} = 5.2 μM; **21F**: EC_{50} = 599 nM). Both EADI and FADI analogues with substitution at the third Lys-Lys showed slightly lower anti-HIV potency than wild-type C29[5] without the α-helix inducible XEEXXKK motifs (**22E**: EC_{50} = 865 nM; **22F**: EC_{50} = 663 nM). The best peptide analogues were obtained by replacement of the C-terminal Lys-Lys with the isosteres (**23E**: EC_{50} = 43 nM; **23F**: EC_{50} = 37 nM); however, the potency was lower than the original SC29EK peptide (EC_{50} = 2.2 nM). Similar bioactivities of peptide **20E–23E** and **20F–23F** were also observed against the other HIV-1 strains (Table 2). These observations suggest that all the peptide bonds within the Lys-Lys and the related H-bonding are essential for the potent anti-HIV activity of SC29EK.

The α-helix properties of these peptides were determined by circular dichroism (CD) analysis (Fig. 2a,b). The stable α-helix

Table 1 Sequences and anti-HIV activities of C29 and its derivatives and T_m values of the mixture with N36

	EADI analogues **E**		FADI analogues **F**	
Sequence[a]	EC_{50} (nM)[b]	T_m (°C)[c]	EC_{50} (nM)[b]	T_m (°C)[c]
WMEWDREINNYTSLIHSLIEESQNQQEKN C29	308 ± 144	51.7	—	—
WEEWDKKIEEYTKKIEELIKKSEEQQKKN SC29EK	2.2 ± 0.2	67.4	—	—
WEEWDKKIEEYTKKIEELIKKSEEQQKKN **20E/20F**	>10000	43.9	5220 ± 202	44.1
WEEWDKKIEEYTKKIEELIKKSEEQQKKN **21E/21F**	>10000	40.1	599 ± 96	49.5
WEEWDKKIEEYTKKIEELIKKSEEQQKKN **22E/22F**	865 ± 317	62.2	663 ± 242	60.9
WEEWDKKIEEYTKKIEELIKKSEEQQKKN **23E/23F**	43 ± 7	64.1	37 ± 6	64.8

[a] The underlined KK dipeptide indicates the position of the dipeptide isostere. [b] EC_{50} was determined as the concentration that blocked HIV-1 (NL4–3 strain) replication by 50%. [c] T_m values were defined by the midpoint of the thermal unfolding transition state as determined from $[\theta]_{222}$ readings.

Table 2 Anti-HIV activities of C29 and its derivatives against three HIV-1 strains

Peptides	EC_{50} (nM)[a]		
	NL4–3	IIIB	Ba-L
C29	308 ± 144	396 ± 83	42 ± 8
SC29EK	2.2 ± 0.2	6.5 ± 0.9	1.9 ± 0.2
20E	>10000	>10000	>10000
20F	5220 ± 202	>10000	5580 ± 1920
21E	>10000	>10000	>10000
21F	599 ± 96	3010 ± 554	600 ± 302
22E	865 ± 317	5110 ± 2,750	2630 ± 386
22F	663 ± 242	2200 ± 712	527 ± 95
23E	37 ± 6	153 ± 27	33 ± 2
23F	43 ± 7	237 ± 16	51 ± 7

[a] EC_{50} is the concentration that blocks HIV-1 replication by 50%.

structure of SC29EK was disrupted by a single substitution of the second or third Lys-Lys peptide bond with the isosteres in **21E/21F** and **22E/22F**. This suggests that the contribution of the H-bonds to the stability of the α-helix is likely to be superior to the multiple introductions of the X-EE-XX-KK motifs at these positions. Conversely, the effects of N- and C-terminal substitution were less significant as observed in **20E/20F** and **23E/23F**. This may be rationalized by the fact that these peptide bonds of SC29EK are positioned at the edge of the helix and that C-terminal Lys-Lys is involved in only upward H-bonding through the donor N–H moiety. CD spectra of SC29EK analogues in the presence of an interactive counterpart N36 indicated the formation of stable six-helix coiled-coil structures (Fig. 2c,d).[13] This observation supports the concept that SC29EK analogues exert their anti-HIV activity by inhibiting the folding process of the HIV-1 envelop protein gp41.

Binding affinity of SC29EK analogues to a viral protein was determined by the thermal stability of the six-helix complexes formed between SC29EK and N36 peptides. The melting temperature (T_m), representing 50% disruption of the six-helix bundle, was comparatively evaluated by monitoring the change in the circular dichroism signal at 222 nm as a function of increasing temperature (Table 1). The complexes involving peptides **20E/20F** and **21E/21F** showed significantly lower thermal stability, which correlates with the observed absent or low anti-HIV activities of these peptides. In contrast, potent analogues **23E/23F** form stable complexes with N36 with T_m values comparable to the value measured for SC29EK (**23E**: T_m = 64.1 °C; **23F**: T_m = 64.8 °C). The N-terminal tryptophan-rich domain (WRD) of inhibitory peptides such as C34 is essential for binding to the cavity formed by the N36 coiled-coil.[11] H-Bonds linked by the first and second Lys-Lys peptide bonds in SC29EK would reinforce the arrangement of these tryptophans. Interestingly, less potent anti-HIV activity of peptide **22E/22F** was observed compared with C29, whereas the complexes with N36 showed higher thermal stability. This result suggests that the loss of crucial H-bonds could reduce the anti-HIV activity, even though the X-EE-XX-KK motifs apparently aid the conformational stability of the six-helix bundle.

In terms of the mimicking ability of the two-peptide-bond isosteres, FADI peptides **20F–23F** exhibited slightly more potent anti-HIV activity and formed more stable complexes with N36 (except for **22F**). Although a fluoroalkene with a large dipole moment imperfectly reproduces the H-bonds needed for α-helix stabilization, FADI is an appropriate peptide bond surrogate to investigate structural requirements in bioactive peptides.

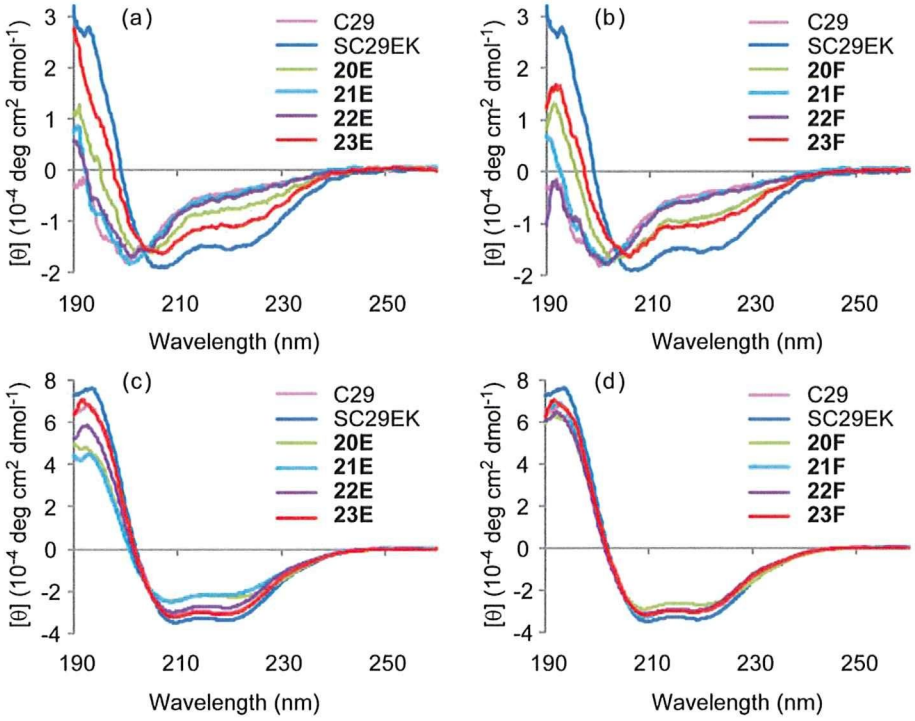

Fig. 2 CD spectra of EADI- and FADI-containing SC29EK analogues in the absence (a,b) and presence (c,d) of N36.

Conclusions

The effects of H-bonds on the stability of the α-helix of an HIV-1 fusion inhibitor were investigated by positional-scanning of the Lys-Lys dipeptides using EADI and FADI. As demonstrated by CD analysis of the SC29EK analogues, H-bonds in the middle of the sequence contribute significantly to the stabilization of the α-helix. In contrast, the effect of H-bonds on the anti-HIV activity of the peptides depends on the distance from the crucial interactive domain. As such, we have shown that EADI and FADI can be used for conformational evaluation of bioactive and/or functional α-helical peptides.

Experimental section

Synthesis

***tert*-Butyl (2*R*,5*S*,3*E*)-2-[4-(*tert*-butyldimethylsiloxy)butyl]-9-[*N*-(2-chlorobenzyloxycarbonyl)amino]-5-[*N*-(2-nitrophenylsulfonyl)amino]non-3-enoate (7).** To a stirred solution of TBSO-$(CH_2)_4$I (236 mg, 0.75 mmol) in dry Et_2O (0.5 cm^3), was added dropwise 1.59 M *t*-BuLi in Et_2O solution (1.0 cm^3, 1.58 mmol) under Ar at −78 °C. After being stirred at this temperature for 30 min, the mixture was stirred at 0 °C for 30 min. To a stirred solution of CuCN (61 mg, 0.61 mmol) and LiCl (52 mg, 1.23 mmol) in dry THF (0.8 cm^3), was added dropwise the above 0.5 M TBSO$(CH_2)_4$Li in THF solution (1.2 cm^3) under Ar at −78 °C, and the mixture was stirred at 0 °C for 10 min. A solution of aziridinyl enoate **6** (91 mg, 0.15 mmol) in dry THF (1.0 cm^3) was added dropwise to the above mixture at −78 °C with stirring, and the stirring was continued for 1.5 h followed by quenching with saturated NH_4Cl/28% NH_4OH solution (1/1, 2.0 cm^3). The mixture was washed with H_2O and brine and dried over $MgSO_4$. Concentration under reduced pressure followed by flash chromatography over silica gel with *n*-hexane-EtOAc (3:1) gave the title compound **7** (72 mg, 60%) as a colorless oil; $[\alpha]^{23}_D$ −73.2 (*c* 0.87 in $CHCl_3$); ν_{max}/cm^{-1} 3349 (NHCO), 1725 (CO); δ_H (500 MHz; $CDCl_3$) 0.04 (6H, s), 0.89 (9H, s), 1.08–1.64 (21H, m), 2.64 (1H, dt, *J* 8.0 and 6.3), 3.07–3.21 (2H, m), 3.55 (2H, t, *J* 6.3), 3.86–3.96 (1H, m), 4.92 (1H, br s), 5.21 (2H, s), 5.26 (1H, dd, *J* 15.5 and 7.5), 5.39 (1H, d, *J* 8.0), 5.40 (1H, dd, *J* 15.5 and 8.0), 7.22–7.30 (2H, m), 7.37 (1H, dd, *J* 5.7 and 2.3), 7.42 (1H, dd, *J* 5.7 and 2.3), 7.65–7.74 (2H, m), 7.83 (1H, dd, *J* 6.9 and 2.3), 8.09 (1H, dd, *J* 6.9 and 2.3); δ_C (100 MHz; $CDCl_3$) −5.3 (2C), 18.3, 22.5, 23.3, 25.9, 28.0 (3C), 29.3 (3C), 32.3, 32.6, 35.4, 40.6, 49.3, 56.7, 62.8, 63.9, 80.6, 125.3, 126.9, 129.3, 129.5, 129.8, 130.9 (2C), 131.2, 132.8, 133.3, 133.5, 134.3, 135.1, 147.8, 156.2, 172.8; *m/z* (FAB) 782.3246 ([M + H]$^+$, $C_{37}H_{57}ClN_3O_9SSi$ requires 782.3273).

(2*R*,5*S*,3*E*)-2-{4-[*N*-(*tert*-Butoxycarbonyl)amino]butyl}-9-[*N*-(2-chlorobenzyloxycarbonyl)amino]-5-[*N*-(9-fluorenylmethoxycarbonyl)amino]non-3-enoic acid (10). To the Fmoc-protected amine **9** (435 mg, 0.52 mmol) was added 4 N HCl/dioxane (5.0 cm^3) at 0 °C, and the mixture was stirred for 20 h at room temperature. Concentration under reduced pressure followed by flash chromatography over silica gel with *n*-hexane-EtOAc (1:1) gave the title compound **10** (391 mg, 96%) as a semisolid; $[\alpha]^{22}_D$ −18.0 (*c* 0.87 in $CHCl_3$); ν_{max}/cm^{-1} 3324 (NHCO), 1703 (CO); δ_H (500 MHz; $CDCl_3$) 1.09–1.81 (12H, m), 2.85–3.01 (1H, m), 3.03–3.21 (4H, m), 4.01–4.21 (2H, m), 4.30–4.54 (2H, m), 4.81–5.26 (6H, m), 5.30–5.81 (3H, m), 7.19–7.41 (13H, m), 7.52–7.59 (2H, m), 7.74 (2H, d, *J* 7.5); δ_C (125 MHz; $CDCl_3$) 22.5, 24.0, 29.2, 29.3, 31.5, 34.3, 40.6 (2C), 47.1, 48.4, 52.3, 63.7, 66.4 (2C), 119.8 (2C), 124.9 (2C), 126.7 (2C), 126.9 (2C), 127.5 (2C), 127.7, 127.9, 128.3, 129.2 (2C), 129.3 (2C), 129.5, 133.3, 134.2, 136.5, 141.1, 143.7 (2C), 143.8 (2C), 155.8, 156.3, 156.4, 178.0; *m/z* (FAB) 782.3201 ([M + H]$^+$, $C_{44}H_{49}ClN_3O_8$ requires 782.3208).

(2*R*,5*S*,3*Z*)-5-[*N*-(*tert*-Butoxycarbonyl)amino]-2-[(*E*)-4-(*tert*-butyldimethylsiloxy)but-2-enyl]-9-(*tert*-butyldimethylsiloxy)-4-fluoronon-3-enoyl (*S*)-sultam (15). To a suspension of CuI (180 mg, 0.94 mmol) in THF (4.8 cm^3) at −78 °C under argon was added dropwise a solution of MeLi·LiBr complex in Et_2O (1.5 M, 1.3 cm^3, 1.89 mmol), and the mixture was stirred for 10 min at 0 °C. To the solution of the above organocopper reagent at −78 °C was added dropwise a solution of the *N*-enoyl sultam **14** (150 mg, 0.24 mmol) in THF (4.8 cm^3). The mixture was stirred for 30 min at −78 °C and HMPA (0.66 cm^3, 3.78 mmol) was added dropwise to the mixture. After stirring for 30 min at −78 °C, a solution of triphenyltin chloride (182 mg, 0.47 mmol) in THF (3.0 cm^3) was added dropwise, and the mixture was then stirred for 30 min at −40 °C. (*E*)-(4-Bromobut-2-enyloxy)(*tert*-butyl)dimethylsilane (501 mg, 1.89 mmol) in THF (3.0 cm^3) was added dropwise and the mixture was stirred for 20 h at −40 °C. The reaction was quenched at −40 °C by addition of a saturated NH_4Cl/28% NH_4OH solution (1/1, 6.0 cm^3) and the mixture was stirred at room temperature for additional 30 min. The mixture was extracted with Et_2O and the extract was washed with brine and dried over $MgSO_4$. Concentration under reduced pressure followed by flash chromatography over silica gel with *n*-hexane-EtOAc (5:1) gave the title compound **15** (148 mg, 78% yield) as a colorless oil; $[\alpha]^{25}_D$ −47.1 (*c* 1.00 in $CHCl_3$); ν_{max}/cm^{-1} 3317 (NHCO), 1693 (CO); δ_H (500 MHz; $CDCl_3$) 0.03 (6H, s), 0.04 (6H, s), 0.88 (9H, s), 0.89 (9H, s), 0.96 (3H, s), 1.15 (3H, s), 1.24–1.64 (17H, m), 1.83–1.91 (3H, m), 2.02–2.05 (2H, m), 2.33–2.37 (1H, m), 2.51–2.55 (1H, m), 3.41 (1H, d, *J* 13.7), 3.49 (1H, d, *J* 13.7), 3.58 (2H, t, *J* 6.3), 3.86 (1H, t, *J* 6.3), 4.06 (2H, d, *J* 3.4), 4.12–4.21 (2H, m), 4.60–4.72 (1H, m), 4.97 (1H, dd, *J* 36.7 and 8.6), 5.58 (2H, m); δ_C (125 MHz; $CDCl_3$) −5.3 (4C), 18.2, 18.3, 19.8, 20.7, 21.9, 25.9 (6C), 26.4, 28.3 (3C), 32.2, 32.3, 32.8, 36.9, 38.3, 41.0, 44.6, 47.6, 48.2, 51.6 (d, *J* 27.6), 53.0, 62.8, 63.5, 65.1, 79.4, 103.3 (d, *J* 12.0), 125.9, 132.7, 154.8, 158.6 (d, *J* 261.5) 172.2; δ_F (470 MHz; $CDCl_3$) −119.1—119.8 (m); *m/z* (FAB) 801.4732 ([M + H]$^+$, $C_{40}H_{74}FN_2O_7SSi_2$ requires 801.4739).

(2*R*,5*S*,3*Z*)-2-{4-[*N*-(Benzyloxycarbonyl)amino]butyl}-9-[*N*-(benzyloxycarbonyl)amino]-5-[*N*-(9-fluorenylmethoxycarbonyl)-amino]-4-fluoronon-3-enoic acid (19). To a solution of the sultam **18** (376 mg, 0.34 mmol) and aqueous 50% H_2O_2 (0.12 cm^3, 1.75 mmol) in THF/H_2O (5/1, 6.0 cm^3) at 0 °C was added aqueous 1 N LiOH (0.67 cm^3, 0.67 mmol), and the mixture was stirred at room temperature for 2 h. After being diluted with EtOAc (20 cm^3), the mixture was washed with 0.1 N HCl and dried over $MgSO_4$. Concentration under reduced pressure gave the corresponding acid, which was used in the next reaction without purification. To a solution of the above acid in CH_2Cl_2 (15 cm^3) at 0 °C was added TFA (4.0 cm^3), and the mixture was stirred at room temperature for 0.5 h. Concentration under reduced pressure gave an oily residue, which was dissolved in MeCN/DMF/H_2O

(10/9/1, 20 cm^3). Fmoc-OSu (159 mg, 0.472 mmol) and Et_3N (0.094 cm^3, 0.675 mmol) were added to the mixture at 0 °C, and the mixture was stirred at room temperature for 12 h. After being diluted with EtOAc (70 cm^3), the reaction mixture was washed with 1 N HCl and dried over $MgSO_4$. Concentration under reduced pressure followed by flash chromatography over silica gel with *n*-hexane-EtOAc (1:1) gave the title compound **19** (267.3 mg, 65% yield) as a semisolid; $[\alpha]^{24}_D$ −19.6 (*c* 1.13 in DMSO); ν_{max}/cm^{-1} 3333 (OH), 1693 (CO); δ_H (500 MHz; DMSO-d_6) 1.04–1.70 (12H, m), 2.89–3.02 (4H, m), 3.21 (1H, dt, *J* 9.7 and 7.5), 3.98–4.10 (1H, m), 4.22 (1H, t, *J* 6.9), 4.30 (2H, d, *J* 6.9), 4.85 (1H, dd, *J* 37.2 and 9.7), 4.99 (4H, s), 7.19–7.44 (16H, m), 7.65–7.74 (3H, m), 7.89 (2H, d, *J* 7.5), 12.35 (1H, br s); δ_C (125 MHz; DMSO-d_6) 22.6, 23.7, 28.9, 29.0, 30.9, 31.9, 40.0, 40.1, 40.3, 46.6, 51.3 (d, *J* 31.2), 65.0, 65.1, 65.4, 104.0 (d, *J* 12.0), 120.0 (2C), 125.1 (2C), 127.0 (2C), 127.6 (2C), 127.6 (4C), 127.7 (2C), 128.3 (4C), 137.2 (2C), 140.7 (2C), 143.7, 143.8, 155.6, 156.0 (2C), 159.4 (d, *J* 257.9), 174.4; δ_F (470 MHz; DMSO-d_6) −117.9–−118.5 (m); *m/z* (FAB) 766.3512 ($[M + H]^+$, $C_{44}H_{49}FN_3O_8$ requires 766.3504).

General procedure for preparation of peptide by Fmoc-SPPS

The protected peptide chains were constructed on the Novasyn® TGR resin (0.26 mmol g^{-1}, 96 mg, 0.025 mmol). *t*-Bu ester for Asp and Glu; 2,2,4,6,7-pentamethyldihydrobenzofuran-5-sulfonyl (Pbf) for Arg; *t*-Bu for Thr, Tyr and Ser; Boc for Lys; and Trt for Gln, Asn and His were employed for side-chain protection. Fmoc-amino acids (0.075 mmol) were coupled by using *N*,*N*′-diisopropylcarbodiimide (DIC; 0.012 cm^3, 0.075 mmol) and *N*-hydroxybenzotriazole monohydrate (HOBt·H_2O, 11.5 mg, 0.075 mmol) in DMF for 2 h. Coupling of dipeptide isosteres (EADI **10**: 49 mg, 0.063 mmol; FADI **19**, 48 mg, 0.063 mmol) was carried out with DIC and HOBt·H_2O for 12 h. The peptide resins were treated with 1 M TMSBr-thioanisole/TFA in the presence of *m*-cresol and 1,2-ethanedithiol as scavengers. The reaction mixture was precipitated with diethyl ether. The resulting powder was collected by centrifugation and then washed three times with diethyl ether. The crude product was purified by preparative HPLC to afford the expected peptides as a colorless powder. The purity of each compound was assessed analytical RP-HPLC prior to the CD analysis and biological testing (>98%).

Anti-HIV-1 activity

Anti-HIV-1 activity was determined by the multinuclear activation of a galactosidase indicator (MAGI) assay as described previously.[14] Briefly, the MAGI cells (10^4 cells $well^{-1}$) were seeded in flat-bottom 96-well microtitre plates. The following day, the cells were inoculated with HIV-1 (60 MAGI units/well, yielding 60 blue cells after 48 h incubation) and cultured in the presence of various concentrations of peptide inhibitors in fresh medium. After 48 h incubation, all the blue cells stained with 5-bromo-4-chloro-3-indolyl-β-D-galactopyranoside (X-gal) in each well were counted. The activity of inhibitors was determined as the concentration that blocked HIV-1 replication by 50% (50% effective concentration [EC_{50}]).

Measurement of CD spectra

Peptides were incubated at 37 °C for 30 min (the final concentrations of peptides were 10 μM in 5 mM HEPES buffer, pH 7.2). CD spectra were acquired on a Jasco spectropolarimeter (Model J-710, Jasco Inc., Tokyo, Japan) at 25 °C as the average of 8 scans. Thermal unfolding at intervals of 0.5 °C was performed after a 0.25-min equilibration at the desired temperature and an integration time of 1.0 s. The mid point of the thermal unfolding transition (melting temperature, T_m) of each complex was determined from the maximum of the first derivative, with respect to the reciprocal of the temperature, of the $[\theta]_{222}$ values.

Acknowledgements

This work was supported by the Science and Technology Incubation Program in Advanced Regions from Japan Science and Technology Agency, Grant-in-Aids for Scientific Research from MEXT, Japan, and Health and Labour Sciences Research Grants (Research on HIV/AIDS). K.T. and T.N. are grateful for the JSPS Research Fellowships for Young Scientists.

References

1 For review, see: J. M. Davis, L. K. Tsou and A. D. Hamilton, *Chem. Soc. Rev.*, 2007, **36**, 326–334.
2 For recent reviews, see: (*a*) J. Garner and M. M. Harding, *Org. Biomol. Chem.*, 2007, **5**, 3577–3585; (*b*) L. K. Henchey, A. L. Jochim and P. S. Arora, *Curr. Opin. Chem. Biol.*, 2008, **12**, 692–697.
3 T. Matthews, M. Salgo, M. Greenberg, J. Chung, R. DeMasi and D. Bolognesi, *Nat. Rev. Drug Discovery*, 2004, **3**, 215.
4 (*a*) A. Otaka, M. Nakamura, D. Nameki, E. Kodama, S. Uchiyama, S. Nakamura, H. Nakano, H. Tamamura, Y. Kobayashi, M. Matsuoka and N. Fujii, *Angew. Chem., Int. Ed.*, 2002, **41**, 2937; (*b*) S. Oishi, S. Ito, H. Nishikawa, K. Watanabe, M. Tanaka, H. Ohno, K. Izumi, Y. Sakagami, E. Kodama, M. Matsuoka and N. Fujii, *J. Med. Chem.*, 2008, **51**, 388–391; (*c*) H. Nishikawa, S. Nakamura, E. Kodama, S. Ito, K. Kajiwara, K. Izumi, Y. Sakagami, S. Oishi, T. Ohkubo, Y. Kobayashi, A. Otaka, N. Fujii and M. Matsuoka, *Int. J. Biochem. Cell Biol.*, 2009, **41**, 891.
5 (*a*) H. Nishikawa, S. Oishi, M. Fujita, K. Watanabe, R. Tokiwa, H. Ohno, E. Kodama, K. Izumi, K. Kajiwara, T. Naitoh, M. Matsuoka, A. Otaka and N. Fujii, *Bioorg. Med. Chem.*, 2008, **16**, 9184–9187; (*b*) T. Naito, K. Izumi, E. Kodama, Y. Sakagami, K. Kajiwara, H. Nishikawa, K. Watanabe, S. G. Sarafianos, S. Oishi, N. Fujii and M. Matsuoka, *Antimicrob. Agents Chemother.*, 2009, **53**, 1013–1018.
6 Recent applications of alkene dipeptide isosteres: (*a*) C. L. Jenkins, M. M. Vasbinder, S. J. Miller and R. T. Raines, *Org. Lett.*, 2005, **7**, 2619–2622; (*b*) J. Xiao, B. Weisblum and P. Wipf, *J. Am. Chem. Soc.*, 2005, **127**, 5742–5743; (*c*) S. Oishi, K. Miyamoto, A. Niida, M. Yamamoto, K. Ajito, H. Tamamura, A. Otaka, Y. Kuroda, A. Asai and N. Fujii, *Tetrahedron*, 2006, **62**, 1416–1424; (*d*) J. Xiao, B. Weisblum and P. Wipf, *Org. Lett.*, 2006, **8**, 4731–4734; (*e*) N. Dai, X. J. Wang and F. A. Etzkorn, *J. Am. Chem. Soc.*, 2008, **130**, 5396–5397; (*f*) C. E. Jakobsche, G. Peris and S. J. Miller, *Angew. Chem., Int. Ed.*, 2008, **47**, 6707.
7 R. J. Abraham, S. L. R. Ellison, P. Schonholzer and W. A. Thomas, *Tetrahedron*, 1986, **42**, 2101–2110.
8 (*a*) T. Ibuka, K. Nakai, H. Habashita, Y. Hotta, N. Fujii, N. Mimura, Y. Miwa, T. Taga and Y. Yamamoto, *Angew. Chem., Int. Ed. Engl.*, 1994, **33**, 652; (*b*) P. Wipf and P. C. Fritch, *J. Org. Chem.*, 1994, **59**, 4875–4886; (*c*) N. Fujii, K. Nakai, H. Tamamura, A. Otaka, N. Mimura, Y. Miwa, T. Taga, Y. Yamamoto and T. Ibuka, *J. Chem. Soc., Perkin Trans. 1*, 1995, 1359.
9 (*a*) T. Narumi, A. Niida, K. Tomita, S. Oishi, A. Otaka, H. Ohno and N. Fujii, *Chem. Commun.*, 2006, 4720–4722; (*b*) T. Narumi, K. Tomita, E. Inokuchi, K. Kobayashi, S. Oishi, H. Ohno and N. Fujii, *Tetrahedron*, 2008, **64**, 4332–4346.

10 H. Tamamura, A. Omagari, K. Hiramatsu, S. Oishi, H. Habashita, T. Kanamoto, K. Gotoh, N. Yamamoto, H. Nakashima, A. Otaka and N. Fujii, *Bioorg. Med. Chem.*, 2002, **10**, 1417–1426.
11 T. Honda, H. Wakabayashi and K. Kanai, *Chem. Pharm. Bull.*, 2002, **50**, 307–308.
12 H. Sajiki, K. Hattori and K. Hirota, *J. Org. Chem.*, 1998, **63**, 7990–7992.
13 (*a*) D. C. Chan, D. Fass, J. M. Berger and P. S. Kim, *Cell*, 1997, **89**, 263–273; (*b*) D. C. Chan, C. T. Chutkowski and P. S. Kim, *Proc. Natl. Acad. Sci. USA*, 1998, **95**, 15613–15617.
14 (*a*) J. Kimpton and M. Emerman, *J. Virol.*, 1992, **66**, 2232–2239; (*b*) E. I. Kodama, S. Kohgo, K. Kitano, H. Machida, H. Gatanaga, S. Shigeta, M. Matsuoka, H. Ohrui and H. Mitsuya, H., *Antimicrob. Agents Chemother.*, 2001, **45**, 1539–1546.

Bioorganic & Medicinal Chemistry 17 (2009) 4916–4920

Contents lists available at ScienceDirect

Bioorganic & Medicinal Chemistry

journal homepage: www.elsevier.com/locate/bmc

Design and synthesis of membrane fusion inhibitors against the feline immunodeficiency virus

Shinya Oishi [a,*], Yasuyo Kodera [a], Hiroki Nishikawa [a], Hirotaka Kamitani [a], Tsuyoshi Watabe [a], Hiroaki Ohno [a], Tadafumi Tochikura [a], Kazuki Shimane [b], Eiichi Kodama [b,†], Masao Matsuoka [b], Fuminori Mizukoshi [c], Hajime Tsujimoto [c], Nobutaka Fujii [a,*]

[a] Graduate School of Pharmaceutical Sciences, Kyoto University, Sakyo-ku, Kyoto 606-8501, Japan
[b] Laboratory of Virus Control, Institute for Virus Research, Kyoto University, Sakyo-ku, Kyoto 606-8507, Japan
[c] Department of Veterinary Internal Medicine, Graduate School of Agricultural and Life Sciences, The University of Tokyo, 1-1-1 Yayoi, Bunkyo-ku, Tokyo 113-8657, Japan

ARTICLE INFO

Article history:
Received 24 April 2009
Revised 30 May 2009
Accepted 2 June 2009
Available online 6 June 2009

Keywords:
Feline immunodeficiency virus
Fusion inhibitor
α-Helix
Heptad repeat

ABSTRACT

Feline immunodeficiency virus (FIV) is a pathogenic virus that causes an AIDS-like syndrome in the domestic cats. For viral entry and infection, fusion between the virus and the cell membrane is the critical process and this process is mediated by an envelope glycoprotein gp40. We have identified fusion inhibitory peptides from the heptad repeat-2 (HR2) of gp40. Remodeling of the original sequences using α-helix-inducible motifs revealed the interactive residues of gp40. Comparative analysis of HR2 peptides derived from four FIV strains demonstrated that the interactive surface of the Shizuoka strain-derived HR2 peptides provides the highest affinity of all the FIV strains examined.

1. Introduction

Feline immunodeficiency virus (FIV) causes immunodeficiency in domestic cats. The prevalence is very high in many countries.[1] FIV shares a homologous replication cycle and pathological processes with human immunodeficiency virus (HIV) in which a progressive and irreversible depletion of $CD4^+$ T cells leads to an AIDS-like syndrome. FIV is horizontally transmitted by the exposure to virus contained in blood or saliva from infected cats and it can be vertically transmitted from queens to kittens, sharing similar transmission routes with HIV. Consequently, FIV has been used as an animal model for the development of anti-HIV agents.[2]

The cell entry process of viruses including receptor binding and membrane fusion is mediated by the envelope glycoproteins.[3] In the initial stage for productive infection, the FIV surface (SU) glycoprotein attaches to both CD134 and CXCR4.[4] The primary receptor of FIV is CD134 expressed on activated $CD4^+$ T cells in contrast that the primate lentiviruses target CD4. The co-receptor CXCR4 is targeted both by FIV and HIV.[5] The inhibitors of this process such as specific CXCR4 antagonists effectively suppress viral replication.[5b,6] Fusion between the host cellular and viral membranes occurs through the rearrangement of the transmembrane (TM) glycoprotein gp40.[7] Although the detailed mechanism of the fusion process of FIV remains unresolved, the conservation of the gp40 ectodomain among the lentiviruses supports the class I membrane fusion reaction. The folding of two heptad repeats in gp40 leads to the formation of a trimer of hairpins with a central α-helical coiled-coil that promotes membrane fusion. As recently observed in the successful development of an HIV fusion inhibitor, enfuvirtide,[8] the fusion process is another promising target for anti-FIV agents.[9]

Recently, we have reported the identification of two potent HIV fusion inhibitors by the remodeling of HIV-1 gp41-derived peptides.[10] Both peptides were designed by the stabilization of bioactive α-helical conformations of C34 **1** and enfuvirtide, which inhibit the refolding process to produce the fusogenic six-helix bundle structure. Incorporation of the characteristic X–EE–XX–KK repeats (X: the original residue; E: Glu; K: Lys) into the gp41 heptad repeat-2 (HR2) peptides stabilized the α-helix structure by the formation of potential electrostatic interaction between Glu at the *i* position and Lys at the *i* + 4 position. Such peptide stabilization resulted in improved anti-HIV activity. In addition, this approach simultaneously distinguished the indispensable residues located at the interactive surface from the less essential solvent accessible residues. These residues can be substituted for improving the aqueous solubility of the peptides. We speculate that this design

* Corresponding authors. Tel.: +81 75 753 4551; fax: +81 75 753 4570.
E-mail addresses: soishi@pharm.kyoto-u.ac.jp (S. Oishi), nfujii@pharm.kyoto-u.ac.jp (N. Fujii).
† Present address: Division of Emerging Infectious Diseases, Tohoku University School of Medicine, 2-1 Seiryocho, Aoba-ku, Sendai 980-8575, Japan.

0968-0896/$ - see front matter © 2009 Elsevier Ltd. All rights reserved.
doi:10.1016/j.bmc.2009.06.001

concept should be applicable to anti-FIV peptides. Since there have been no previous reports on the interactive mode of FIV gp40 during the fusion process, this approach could identify novel potent anti-FIV peptides and disclose the interacting interface for further optimization.

Herein, we present the design, synthesis and bioevaluation of FIV HR2-derived peptides with α-helix inducible motifs. On the basis of the appropriate anti-FIV sequence identified, the congeneric HR2 peptides from four FIV strains belonging to two different subtypes were comparatively evaluated for inhibitory activity against the fusion process by using an ELISA.

2. Results and discussion

2.1. Peptide design and synthesis

Peptide design began with two putative coiled-coil-like regions of FIV envelope protein gp40 identified by the LearnCoil-VMF program.[11] Alignment with two heptad repeats of HIV-1 gp41 identified the corresponding heptad repeat-1 (HR1) and HR2 regions in FIV gp40 (Fig. 1a).[11] The predicted C-terminal sequence **3a** coincides with a previously reported effective inhibitor of FIV infection, T1577,[9b] and shares four amino acids with HR2 of HIV-1 gp41. The potential α-helical wheel of **3a** is depicted in Figure 1b. On the basis of the crystal structure of HIV-1 gp41 and the alignment with the HIV-1 sequence, it is assumed that residues at the *a*, *d* and *e* positions of peptide **3a** are involved in the interaction with the central coiled-coil of the HR1 trimer to form the six-helix bundle. On the other hand, residues at *b*, *c*, *f* and *g* positions may facilitate the stabilization of the bioactive secondary structure rather than directly interact with HR1. We designed a modified peptide **4a**, in which Glu and Lys were arranged for *b*/*c* and *f*/*g* positions of **3a**, respectively, in order to stabilize the α-helix structure through the formation of consecutive salt bridges. In addition, two analogues **5** and **6** with shifted interactive surfaces were designed, in which *a*/*b*/*e* and *a*/*d*/*g* positions were expected to interact with HR1, respectively.

All peptides were prepared by a standard protocol for Fmoc-based solid-phase peptide synthesis. The peptide resins were manually constructed using *N*,*N*-diisopropylcarbodiimide (DIC) and *N*-hydroxybenzotriazole (HOBt) on NovaSyn TGR resin. The peptide N-terminus was acetylated. The peptides were obtained by the treatment with the deprotection cocktail [TFA/thioanisole/*m*-cresol/1,2-ethanedithiol/H_2O (80:5:5:5:5)] followed by HPLC purification. The peptides were characterized by mass spectrometry.

2.2. Identification of the interactive surface of HR2 for binding with the HR1 core

The inhibitory potency of HR2 peptides against the six-helix bundle formation of FIV gp40 was examined by an ELISA (Table 1).[12] Two peptides **4a** and **5** exhibited higher inhibition compared with the parent peptide **3a** [IC_{50}(**3a**) = 708 nM; IC_{50}(**4a**) = 16.6 nM; IC_{50}(**5**) = 169 nM], whereas peptide **6** did not inhibit the interaction even at 10 μM. HIV fusion inhibitors C34 **1** and SC35EK **2** showed no inhibition. These results indicate that the FIV HR2 sequence may interact with the HR1 coiled-coil via the residues positioned at *a*/*b*/*e* and/or *a*/*d*/*e*. On the other hand, FIV-mediated syncytium formation and FIV replication were blocked by treatment with peptides **3a** and **4a**, but not by peptides **5** and **6**.[13] Inhibition of the HR1–HR2 interaction by peptide **5** did not lead to anti-FIV activity suggesting that residues at *d* position are required for the interaction with HR1 of FIV gp40.

In order to rationalize the relationship between bioactivity and the conformations of the HR2 peptides, circular dichroism (CD) spectra were measured for peptides **3a, 4a, 5** and **6** in the absence or presence of the HR1 peptide. Negative ellipticities around 208 and 222 nm indicate the presence of a stable α-helix structures for peptides **4a** and **5** in the absence of the HR1 peptide (Fig. 2a). In contrast, although the α-helix inducible motifs were included, a random structure was observed for peptide **6**. The CD spectrum

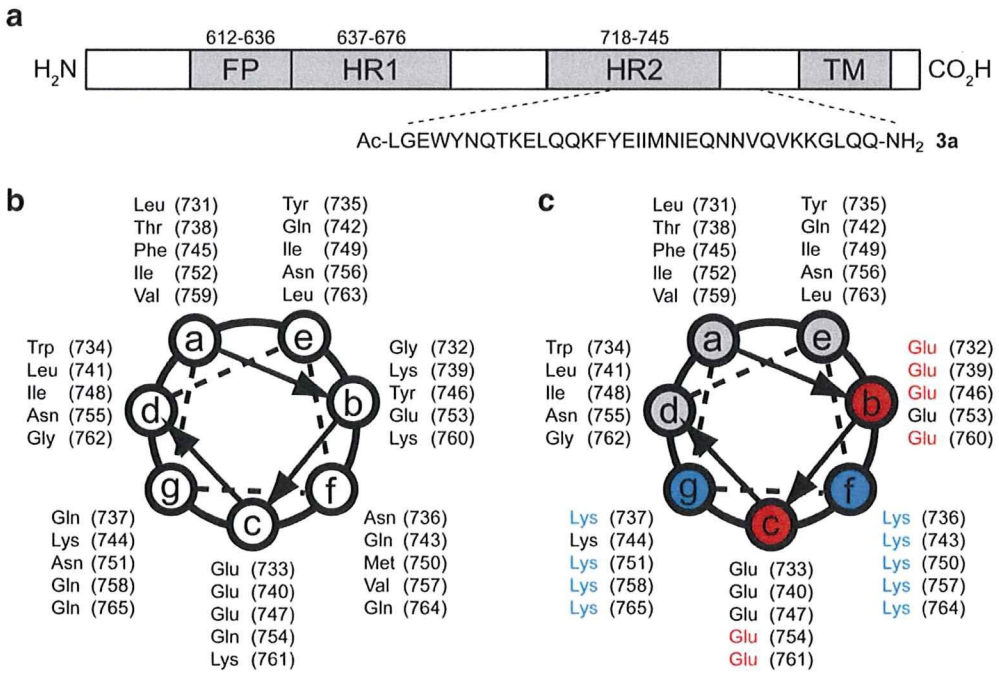

Figure 1. Design of FIV fusion inhibitors. (a) Schematic representation of FIV-1 gp40. The helical wheel representation of the HR2 peptide of FIV-1 gp40: (b) peptide **3a** and (c) peptide **4a**. FP: fusion peptide; HR1: heptad repeat-1; HR2: heptad repeat-2; TM: transmembrane domain.

Table 1
Sequences and bioactivity of HR2-derived peptides of HIV-1 and FIV.

Peptide	Sequence	IC_{50} (nM)[a]
HIV-1		
1 (C34)	WMEWDREINNYTSLIHSLIEESQNQQEKNEQELL	>10,000
2 (SC35EK)	WEEWDKKIEEYTKKIEELIKKSEEQQKKNEEELKK	>10,000
FIV		
3a	LGEWYNQTKELQQKFYEIIMNIEQNNVQVKKGLQQ	708
4a	LEEWYKKTEELQKKFEEIIKKIEENNKKVEEGLKK	16.6
5	NEELGKKYEETKKKQEEFYKKIEEIEKKNEEVKKKLEELQKK	169
6	GEETLKKWEEQTKKLEEKFKKIEENIKKNEEQVKKGEEQLKK	>10,000

[a] IC_{50} was determined as the concentration that blocked HR1–HR2 interaction by 50% in an ELISA.

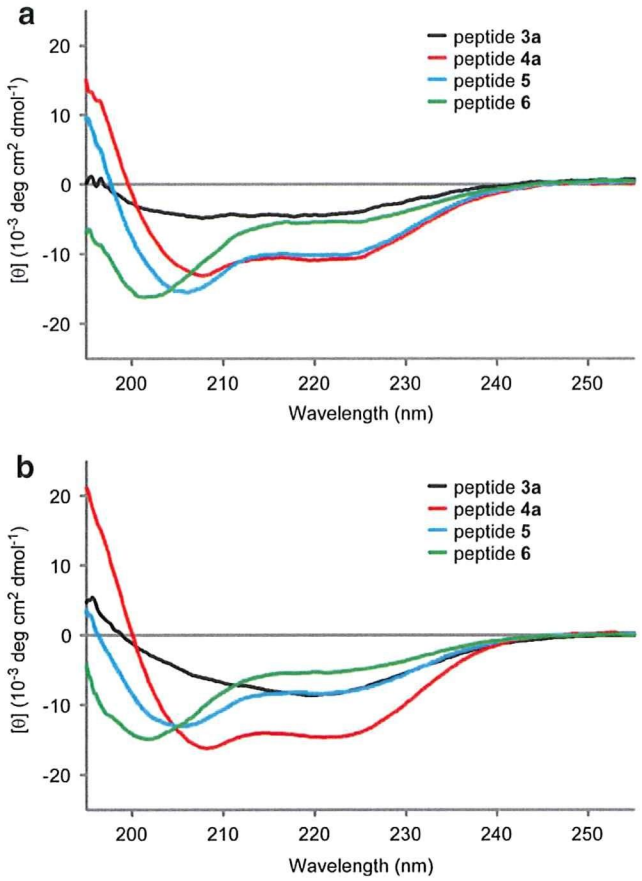

Figure 2. Circular dichroism spectra of HR2 peptides **3a**, **4a**, **5** and **6** in the presence (a) and absence (b) of the HR1 peptide.

of peptide **4a** in the presence of the HR1 peptide showed a slight enhancement of α-helix conformation compared with the theoretical spectrum of the mixture without the interaction between HR1 and HR2 (Fig. 2b). This observation suggests that a stable six-helix bundle structure was formed between HR1 peptide and **4a**. The other HR1–HR2 mixtures did not indicate any enhancement in α-helix content, which is correlated with the results obtained by a replication assay.[13] As such, it was demonstrated that residues at positions *a*/*d*/*e* of peptide **4a** provide the most appropriate interactive surface required for designing inhibitors against FIV infection (Fig. 1c).

2.3. Structure–activity relationship for designing potent fusion inhibitors against multiple FIV strains

The inhibitory potency of the anti-FIV HR2 peptides is affected by both the interactive surface and the stabilized α-helix conformations supported by the arrangement of residues exposed to the aqueous solvent. Since the α-helix content and stability of the peptide was enhanced by the X–EE–XX–KK motifs, the *a*, *d* and *e* positions could be further optimized for improving binding affinity. In addition, considering the clinical application against feline immunodeficiency, inhibitors that potently suppress broad range of FIV strains are favorable. Next, comparative inhibition of analogous peptides **3a–d** (native sequences) and **4a–d** (remodeled sequences) derived from several FIV strains was examined against potential formation of the six-helix bundles (Tables 2 and 3). Noticeably, peptide **3d** from the Shizuoka strain (clade D) contains ten different residues from **3a** (UK8) and **3c** (Sendai-1), and nine from **3b** (Petaluma). In contrast, there are only three differences in residue type observed among remodeled peptides **4a–d**, suggesting that the potential interactive residues are conserved among the four FIV strains.

ELISA with gp40 fragments derived from each strain was performed. Peptides **4a–d** with α-helix inducible motifs exhibited higher potency of inhibition compared with the native sequences **3a–d**. FIV-mediated syncytium formation was also inhibited by peptides **3b** and **4b** (Fig. 3). Sendai-1-derived peptides **3c** and **4c** were less potent compared with the other peptides, suggesting that the N26S substitution on the interactive surface results in a decrease in the affinity towards the HR1 peptide. In contrast, the Shizuoka sequence provided the most potent peptides **3d** and **4d** against all strains. The potent bioactivity was attributed to a combination of Gly and Leu at the positions 29 and 33, respectively. Accordingly, the exposure of appropriate residues on the HR2 interactive surface such as the Shizuoka strain-derived peptide **4d** provide optimized inhibition against the formation of the six-helix bundle.

Comparative CD analysis demonstrated that the sequences of the HR1 peptide apparently influence the structures of the six-helix bundles (Fig. 4a). In contrast, peptides **4a–d** in the presence of an HR1 peptide derived from each strain exhibited similar six-helix bundle structures (Fig. 4b and Supplementary data).[14] These observations suggest that the binding affinity between the viral HR1 peptide and the inhibitory HR2 peptide would be determined primarily by the sequence of the viral HR1 peptide when the HR2 sequence was simplified by the incorporation of α-helix inducible motifs.

Table 2
Sequences of HR2-derived peptides of four FIV strains.

Peptide		Sequence[a]
clade A		1 10 20 30 35
UK8	3a	LGEWYNQTKELQQKFYEIIMNIEQNNVQVKKGLQQ
	4a	LEEWYKKTEELQKKFEEIIKKIEENNKKVEEGLKK
Petaluma	3b	LGEWYNQTKDLQQKFYEIIMDIEQNNVQGKKGIQQ
	4b	LEEWYKKTEELQKKFEEIIKKIEENNKKGEEGIKK
Sendai-1	3c	LGEWYNQTKGLQQKFYEIIMDIEQNSVQGKKGIQQ
	4c	LEEWYKKTEELQKKFEEIIKKIEENSKKGEEGIKK
clade D		
Shizuoka	3d	LRDWYNNTQQLQKKFYEIIYDIEQNNVQGKQGLQQ
	4d	LEEWYKKTEELQKKFEEIIKKIEENNKKGEEGLKK

[a] The different residues in peptides **4b–d** from peptide **4a** are marked in green.

Table 3
Inhibitory activity of HR2-derived peptides against the HR1–HR2 interaction of four FIV strains

Peptide	IC_{50} (nM, ELISA)[a]			
	UK8	Petaluma	Sendai-1	Shizuoka
3a	724	708	646	6310
3b	513	1260	183	6310
3c	>10,000	2400	437	>10,000
3d	182	195	37.2	2510
4a	5.39	16.6	22.6	115
4b	9.33	51.6	8.87	78.5
4c	443	200	42.4	203
4d	3.38	12.8	2.53	19.7

[a] IC_{50} was determined as the concentration that blocked HR1–HR2 interaction by 50% in an ELISA.

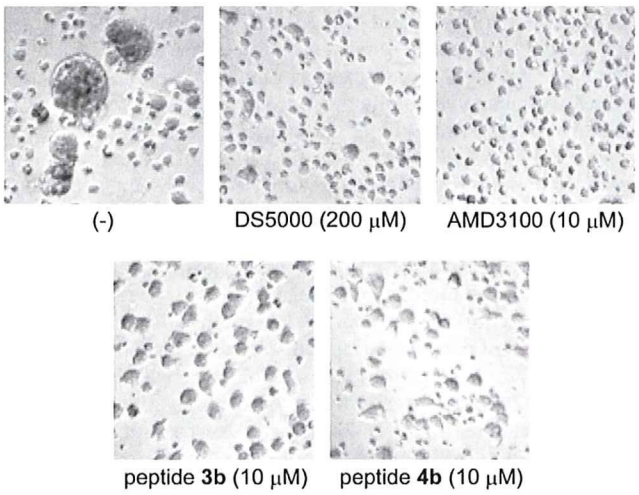

Figure 3. Inhibition of FIV-mediated cell fusion by peptides **3b** and **4b**.

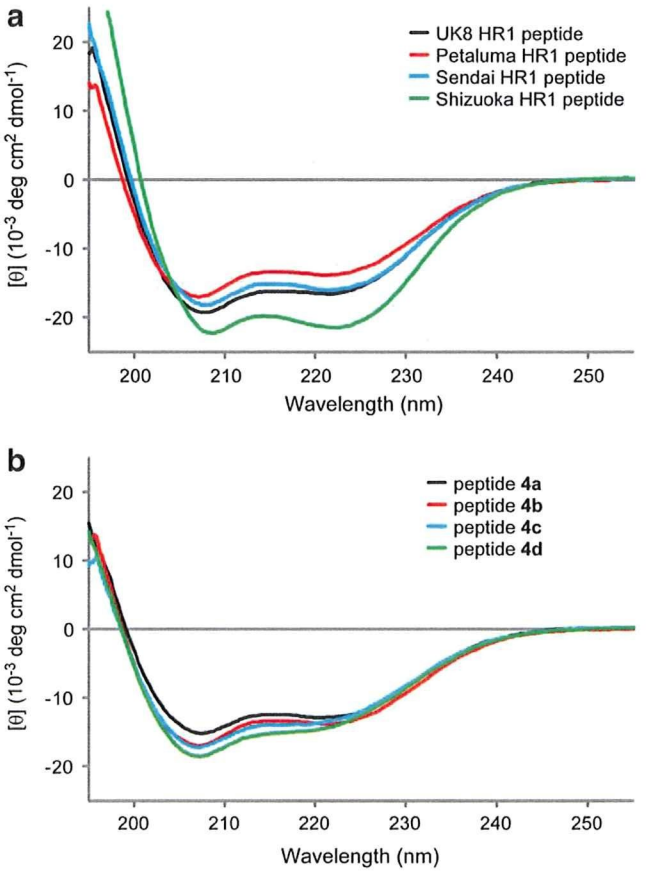

Figure 4. Circular dichroism spectra of (a) peptide **4a** in the presence of HR1 peptides (four strains) and (b) peptides **4a–d** in the presence of the HR1 peptide (Petaluma strain).

3. Conclusions

The current study investigated the use of an α-helix inducible X–EE–XX–KK motif to stabilize the interaction between HR2 and the HR1 coiled-coil of the FIV gp40 protein. The most appropriate interactive surface on the HR2 peptide to provide potent inhibition appeared in the remodeled peptide **4a**, which was designed on the basis of the alignment with the HIV-1 gp41 HR2 sequence. Comparative analysis of HR2 peptides derived from several strains indicated that the most potent inhibition was provided by the interactive residues of the Shizuoka strain-derived peptide **4d**. As such, replacement of the solvent accessible residues with arranged Glu and Lys residues facilitated the optimization process of the interactive residues for high affinity binding on to the HR1 structure. Since class I virus fusion proteins share a high degree of structural homology and similar molecular mechanisms, the current approach may be useful in designing fusion inhibitors against other related viruses.

4. Experimental

4.1. Peptide synthesis

Protected peptide-resins were manually constructed by Fmoc-based solid-phase peptide synthesis on NovaSyn® TGR resin (0.26 mmol/g, 385 mg, 0.1 mmol). *t*-Bu ester for Asp and Glu; 2,2,4,6,7-pentamethyldihydrobenzofuran-5-sulfonyl (Pbf) for Arg; *t*-Bu for Thr, Tyr and Ser; Boc for Lys; and Trt for Gln, Asn and His were employed for side-chain protection. Fmoc-amino acids were coupled using Fmoc-amino acid (0.5 mmol), *N*,*N*′-diisopropylcarbodiimide (DIC, 0.077 mL, 0.5 mmol) and HOBt·H_2O (77 mg) in DMF for 1.5 h. Fmoc deprotection was performed with 20% piperidine in DMF for 20 min. After N-terminal acetyl capping by treatment with Ac_2O (0.050 mL)-pyridine (0.050 mL), the protected resin (200 mg) was treated with TFA/thioanisole/*m*-cresol/1,2-ethandithiol/H_2O (80:5:5:5:5, 2.5 mL) at room temperature for 2 h. After removal of the resin by filtration, the filtrate was poured into ice-cold dry Et_2O. The resulting powder was collected by centrifugation and washed with ice-cold dry diethyl ether. Purification of the crude product by preparative HPLC on a Cosmosil 5C18-ARII preparative column (Nacalai Tesque, 20 × 250 mm) afforded the expected peptides. All peptides were characterized by an ESI-MS (Sciex API*III*E, Toronto, Canada) or MALDI-TOF-MS (AXIMA-CFR plus, Shimadzu, Kyoto, Japan), and the purity was calculated as >95% by HPLC on a Cosmosil 5C18-ARII analytical column (Nacalai Tesque, 4.6 × 250 mm) at 220 nm absorbance. The MS data are shown in Supplementary data.

4.2. FIV syncytial assay[15]

3201/FIV cells (2×10^4 cells/well) and MT-2 cells (1×10^3 cells/well) were seeded into 96-well plates with each peptide (10 μM). After 7 days, the cells were fixed with 1% formaldehyde and were examined using a BioZERO microscope (BZ-8000; Keyence, Osaka, Japan).

4.3. ELISA-based competition assay

Recombinant purified MBP-HR1 dissolved in 50 mM sodium carbonate buffer (pH 8.5) was coated on a 96-well ELISA plate

(Costar, Cambridge, MA) by incubation at 4 °C for 12 h. After washing three times with PBS containing 0.25% Tween 20 (T-PBS), the plate was blocked using bovine serum albumin (BSA) at a concentration of 1 mg/mL in T-PBS at 4 °C for 2.5 h, and then washed again as described above. The MBP-HR1 was allowed to bind biotinylated HR2 peptide (peptide **3**, 120 nM) by incubation at 37 °C for 1.5 h in the presence or absence of various concentrations of the test peptides. After washing, binding of biotin-HR2 peptide was detected using streptavidin alkaline phosphatase (CALBIOCHEM) using a 1:5000 dilution at 4 °C for 1 h. Subsequently, this reaction was washed as before, prior to the addition of the phosphatase substrate 5-bromo-4-chloro-3-indolyl phosphate (BCIP) (BluePhos Microwell Phosphatase Substrate; KPL, Gaithersburg, MD). After incubating at room temperature for 25 min, the absorbance at 595 nm was measured using a plate reader (Model 3550, Bio-Rad).

4.4. Measurement of CD spectra

The HR2 peptide was dissolved in PBS (pH 7.4) at a concentration of 10 μM. The mixture of the selected HR1 and HR2 peptides was incubated at 37 °C for 30 min prior to the CD measurement (the final concentration of both HR1 and HR2 peptides was 10 μM in PBS, pH 7.4). The wavelength-dependent molar ellipticity $[\theta]$ was monitored at 25 °C as the average of eight scans, and the thermal stability of the HR1 and HR2 mixture was estimated by monitoring the change in the CD signal at 222 nm in a spectropolarimeter (Model J-710; Jasco, Tokyo, Japan). The midpoint of the thermal unfolding transition of each complex was defined as the melting temperature (T_m).

Acknowledgments

This work was supported by the Science and Technology Incubation Program in Advanced Regions from the Japan Science and Technology Agency, Grants-in-Aid for Scientific Research from the Ministry of Education, Culture, Sports, Science, and Technology of Japan, and Health and Labour Sciences Research Grants (Research on HIV/AIDS). H.N. is grateful for the JSPS Research Fellowships for Young Scientists.

Supplementary data

Supplementary data associated with this article can be found, in the online version, at doi:10.1016/j.bmc.2009.06.001.

References and notes

1. Dunham, S. P.; Graham, E. *Vet. Clin. Small Anim. Pract.* **2008**, *38*, 879.
2. Fletcher, N. F.; Brayden, D. J.; Brankin, B.; Callanan, J. J. *Vet. Immunol. Immunopathol.* **2008**, *123*, 134.
3. (a) Wyatt, R.; Sodroski, J. *Science* **1998**, *280*, 1884; (b) Garg, H.; Fuller, F. J.; Tompkins, W. A. *Virology* **2004**, *321*, 274; (c) Elder, J. H.; Sundstrom, M.; De Rozieres, S.; De Parseval, A.; Grant, C. K.; Lin, Y. C. *Vet. Immunol. Immunopathol.* **2008**, *123*, 3.
4. (a) Shimojima, M.; Miyazawa, T.; Ikeda, Y.; McMonagle, E. L.; Haining, H.; Akashi, H.; Takeuchi, Y.; Hosie, M. J.; Willett, B. J. *Science* **2004**, *303*, 1192; (b) De Parseval, A.; Chatterji, U.; Sun, P.; Elder, J. H. *Proc. Natl. Acad. Sci. U.S.A.* **2004**, *101*, 13044.
5. (a) Willett, B. J.; Hosie, M. J.; Neil, J. C.; Turner, J. D.; Hoxie, J. A. *Nature* **1997**, *385*, 587; (b) Richardson, J.; Pancino, G.; Merat, R.; Leste-Lasserre, T.; Moraillon, A.; Schneider-Mergener, J.; Alizon, M.; Sonigo, P.; Heveker, N. *J. Virol.* **1999**, *73*, 3661.
6. (a) Egberink, H. F.; De Clercq, E.; Van Vliet, A. L.; Balzarini, J.; Bridger, G. J.; Henson, G.; Horzinek, M. C.; Schols, D. *J. Virol.* **1999**, *73*, 6346; (b) Mizukoshi, F.; Baba, K.; Goto-Koshino, Y.; Setoguchi-Mukai, A.; Fujino, Y.; Ohno, K.; Tamamura, H.; Oishi, S.; Fujii, N.; Tsujimoto, H. *J. Vet. Med. Sci.* **2009**, *71*, 121.
7. Kielian, M.; Rey, F. A. *Nat. Rev. Microbiol.* **2006**, *4*, 67.
8. Matthews, T.; Salgo, M.; Greenberg, M.; Chung, J.; DeMasi, R.; Bolognesi, D. *Nat. Rev. Drug Discovery* **2004**, *3*, 215.
9. (a) Lombardi, S.; Massi, C.; Indino, E.; La Rosa, C.; Mazzetti, P.; Falcone, M. L.; Rovero, P.; Fissi, A.; Pieroni, O.; Bandecchi, P.; Esposito, F.; Tozzini, F.; Bendinelli, M.; Garzelli, C. *Virology* **1996**, *220*, 274; (b) Medinas, R. J.; Lambert, D. M.; Tompkins, W. A. *J. Virol.* **2002**, *76*, 9079; (c) D'Ursi, A. M.; Giannecchini, S.; Di Fenza, A.; Esposito, C.; Armenante, M. R.; Carotenuto, A.; Bendinelli, M.; Rovero, P. *J. Med. Chem.* **2003**, *46*, 1807; (d) Giannecchini, S.; Di Fenza, A.; D'Ursi, A. M.; Matteucci, D.; Rovero, P.; Bendinelli, M. *J. Virol.* **2003**, *77*, 3724; (e) Giannecchini, S.; Alcaro, M. C.; Isola, P.; Sichi, O.; Pistello, M.; Papini, A. M.; Rovero, P.; Bendinelli, M. *Antiviral Ther.* **2005**, *10*, 671; (f) D'Ursi, A. M.; Giannecchini, S.; Esposito, C.; Alcaro, M. C.; Sichi, O.; Armenante, M. R.; Carotenuto, A.; Papini, A. M.; Bendinelli, M.; Rovero, P. *Chembiochem.* **2006**, *7*, 774.
10. (a) Otaka, A.; Nakamura, M.; Nameki, D.; Kodama, E.; Uchiyama, S.; Nakamura, S.; Nakano, H.; Tamamura, H.; Kobayashi, Y.; Matsuoka, M.; Fujii, N. *Angew. Chem., Int. Ed.* **2002**, *41*, 2937; (b) Oishi, S.; Ito, S.; Nishikawa, H.; Watanabe, K.; Tanaka, M.; Ohno, H.; Izumi, K.; Sakagami, Y.; Kodama, E.; Matsuoka, M.; Fujii, N. *J. Med. Chem.* **2008**, *51*, 388; (c) Nishikawa, H.; Oishi, S.; Fujita, M.; Watanabe, K.; Tokiwa, R.; Ohno, H.; Kodama, E.; Izumi, K.; Kajiwara, K.; Naitoh, T.; Matsuoka, M.; Otaka, A.; Fujii, N. *Bioorg. Med. Chem.* **2008**, *16*, 9184; (d) Nishikawa, H.; Nakamura, S.; Kodama, E.; Ito, S.; Kajiwara, K.; Izumi, K.; Sakagami, Y.; Oishi, S.; Ohkubo, T.; Kobayashi, Y.; Otaka, A.; Fujii, N.; Matsuoka, M. *Int. J. Biochem. Cell Biol.* **2009**, 891; (e) Naito, T.; Izumi, K.; Kodama, E.; Sakagami, Y.; Kajiwara, K.; Nishikawa, H.; Watanabe, K.; Sarafianos, S. G.; Oishi, S.; Fujii, N.; Matsuoka, M. *Antimicrob. Agent Chemother.* **2009**, *53*, 1013.
11. Singh, M.; Berger, B.; Kim, P. S. *J. Mol. Biol.* **1999**, *290*, 1031.
12. Nishikawa, H.; Kodama, E.; Sakakibara, A.; Fukudome, A.; Izumi, K.; Oishi, S.; Fujii, N.; Matsuoka, M. *Antiviral Res.* **2008**, *80*, 71.
13. Mizukoshi, F.; Baba, K.; Goto, Y.; Setoguchi, A.; Fujino, Y.; Ohno, K.; Oishi, S.; Kodera, Y.; Fujii, N.; Tsujimoto, H. *Vet. Microbiol.* **2009**, *136*, 155.
14. The similar thermal stabilities of the potential six-helix bundle structures were also observed. For example, the melting temperatures (T_m) of peptides **4c** and **4d** in the presence of UK8 strain-derived HR1 peptide were 57.1 °C and 54.7 °C, respectively. Unfortunately, we were not able to get clearer physicochemical proofs of the lower bioactivity of the Sendai strain-derived peptide **4c**.
15. Tanabe-Tochikura, A.; Tochikura, T. S.; Blakeslee, J. R., Jr.; Olsen, R. G.; Mathes, L. E. *Antiviral. Res.* **1992**, *19*, 161.

doi:10.1016/j.jmb.2009.07.027 J. Mol. Biol. (2009) 392, 657–665

JMB

Available online at www.sciencedirect.com

ScienceDirect

ELSEVIER

X-ray Crystallographic Study of an HIV-1 Fusion Inhibitor with the gp41 S138A Substitution

Tsuyoshi Watabe[1], Yukihiro Terakawa[1], Kentaro Watanabe[1], Hiroaki Ohno[1], Hiroaki Nakano[1], Toru Nakatsu[1], Hiroaki Kato[1], Kazuki Izumi[2], Eiichi Kodama[2], Masao Matsuoka[2], Kazuo Kitaura[1], Shinya Oishi[1]* and Nobutaka Fujii[1]*

[1]*Graduate School of Pharmaceutical Sciences, Kyoto University, Sakyo-ku, Kyoto 606-8501, Japan*

[2]*Institute for Virus Research, Kyoto University, Sakyo-ku, Kyoto 606-8507, Japan*

Received 28 March 2009; received in revised form 6 July 2009; accepted 8 July 2009
Available online 17 July 2009

Edited by I. Wilson

The S138A substitution of fusion inhibitory peptides derived from the C-terminal heptad repeat (C-HR) of the human immunodeficiency virus type 1 (HIV-1) gp41 leads to enhanced binding affinity to the N-terminal heptad repeat (N-HR). As such, these peptides exhibit highly potent anti-HIV-1 activity. X-ray crystallographic analysis was performed to understand the effect of the substitution on binding affinity. The comparison of the native and S138A crystal structures indicated that the increase in the hydrophobicity of the S138A substitution may aid the stabilization of the N-HR/C-HR complex through additional hydrophobic contacts. Free-energy calculations suggest that the difference between the desolvation free energies of the C-HR-derived peptides with and without the S138A mutation dominates the observed difference in anti-HIV-1 activity.

Keywords: HIV-1 fusion inhibitor; C-HR-derived peptide; gp41/S138A substitution; hydrophobicity; desolvation energy

Introduction

The entry of human immunodeficiency virus type 1 (HIV-1) into host cells is mediated by the formation of the six-helix bundle of the envelope glycoprotein gp41 consisting of several functional domains (Fig. 1), including the N-terminal heptad repeat (N-HR) and C-terminal heptad repeat (C-HR).[1–4] The N-HR trimeric core of the six-helix bundle has been an attractive anti-HIV drug target. Currently, synthetic peptides derived from the C-HR have been shown to be inhibitors against HIV-1 infection.[5–8] One of these peptides, T-20 (enfuvirtide, Fuzeon; corresponding to residues 127 to 162 of the gp41 C-HR), is an approved anti-HIV-1 peptide for clinical use.[8,9] T-20 inhibits HIV-1 entry into host cells and is used as an alternative anti-HIV drug for patients with drug resistance to reverse transcriptase and/or protease inhibitors. However, long-term therapy with T-20 has led to the emergence of T-20-resistant HIV-1 strains containing mutations within the N- and C-HRs of gp41.[10–12] Consequently, the continuous discovery and development of anti-HIV-1 peptides are essential to overcome drug-resistant HIV-1 strains.

Previously, on the basis of the amino acid sequences of C-HR-derived peptides C34 (corresponding to residues 117 to 150 of gp41 C-HR) and T-20, we designed SC35EK and T-20EK as potent HIV-1 fusion inhibitors against wild-type and T-20-resistant HIV-1 strains.[13,14] Here, N-HR/C-HR interfacial residues critical for interaction with the hydrophobic groove of the N-HR trimeric core were preserved, while other residues were replaced with Glu or Lys to strengthen the bioactive α-helix structure via the formation of potential salt bridges. Other groups have reported that C-HR-derived peptides containing various α-helix-inducible motifs increase peptide bioactivity.[15,16] Although these studies have been successful in producing potent HIV-1 fusion inhibitors, the precise structural analysis are required for improving the N-HR/C-

**Corresponding authors.* E-mail addresses: soishi@pharm.kyoto-u.ac.jp; nfujii@pharm.kyoto-u.ac.jp.

Abbreviations used: HIV-1, human immunodeficiency virus type 1; N-HR, N-terminal heptad repeat; C-HR, C-terminal heptad repeat; MAGI, multinuclear activation of the galactosidase indicator; MM, molecular mechanics; PBSA, Poisson–Boltzmann surface area; PDB, Protein Data Bank.

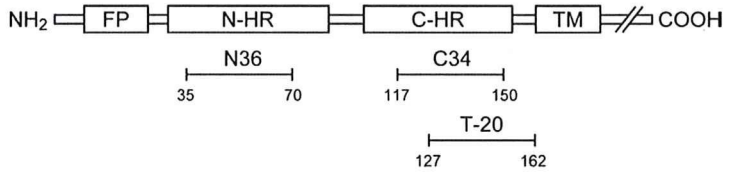

N36: SGIVQQQNNLLRAIEAQQHLLQLTVWGIKQLQARIL

C34: WMEWDREINNYTSLIHSLIEESQNQQEKNEQELL

T-20: YTSLIHSLIEESQNQQEKNEQELLELDKWASLWNWF

Fig. 1. Schematic representation of HIV-1 gp41 (FP, fusion peptide region; TM, transmembrane domain). Peptides N36, C34, and T-20 correspond to residues 35–70, 117–150, and 127–162, respectively. The residues are numbered starting at the first amino acid of the NL4-3 (GIV) gp41.

HR interactions and further peptide and/or non-peptide drug developments.

Currently, the structure–activity relationship studies of an N-HR/C-HR interfacial residue Trp120 in the C-HR-derived peptide C34 were carried out *in vitro* and *in silico*.[17,18] These studies serve as a useful basis for rational drug design targeting the conserved hydrophobic pocket of the N-HR trimeric core. In addition, we have performed an *in vitro* structure–activity relationship study of another residue (i.e., Ser138) located within the N-HR/C-HR binding interface using the C-HR-derived peptides T-20 and C34.[19] Ser138 has been identified to interact within the neighborhood of the primary T-20-resistant mutation region (Leu33-Leu45 of the N-HR), and chemical modification of this residue should improve binding with the T-20-resistant N-HR mutants. We demonstrated that mutation of Ser138 with a small or hydrophobic amino acid enhanced T-20 activity against the wild-type HIV-1. Moreover, the substitution to Ala (T-20_{S138A}) inhibited replication of T-20-resistant clones (HIV-1_{V38A}, HIV-1_{N43D}, and HIV-$1_{N43D/S138A}$) as efficiently as the wild-type HIV-1. In this article, we have determined the X-ray crystal structure of the N36/$C34_{S138A}$ complex to compare this structure with the previously reported structure of the N36/C34 complex [Protein Data Bank (PDB) code: 1AIK] and evaluate the effect of the S138A substitution. Based on the X-ray coordinates, the binding energies of C34 and $C34_{S138A}$ to the gp41 N-HR were calculated using molecular mechanics (MM) and Poisson–Boltzmann surface area (PBSA) solvation modeling.[20]

Results and Discussion

Anti-HIV-1 activities and thermal stabilities of C-HR-derived peptides

Anti-HIV-1 activities of C-HR-derived peptides (C34 and $C34_{S138A}$) against laboratory HIV-1 NL4-3 (GIV) were evaluated using the multinuclear activation of the galactosidase indicator (MAGI) assay (Table 1).[19] Although original NL4-3 contains D36 substitution,[21] vast majority of HIV-1 strains do G36. Therefore, we used NL4-3(GIV) clone in this study. $C34_{S138A}$ exhibited approximately 4-fold greater anti-HIV-1 activity than C34 [C34, 50% effective concentration (EC_{50}) = 7.3 ± 2.5 nM; $C34_{S138A}$, EC_{50} = 2.0 ± 0.4 nM]. Consequently, the S138A substitution enhanced the C34 activity against the HIV-1 NL4-3(GIV) strain.

The anti-HIV-1 activities of the C-HR-derived peptides have been reported to directly correlate with the apparent melting temperatures (T_m) for the N-HR/C-HR complexes.[17,22,23] As shown in Table 1, the complex containing the $C34_{S138A}$ peptide exhibited a higher T_m value than the complex containing the C34 peptide (N36/C34, T_m = 67.6 °C; N36/$C34_{S138A}$, T_m = 73.2 °C). This observation is in agreement with previous results examining C-HR-derived peptides.

Experimental binding energies (ΔG_{bind} exptl) of the C-HR-derived peptides to the gp41 N-HR have been estimated using the IC_{50} values via ΔG_{bind} exptl $\approx RT\ln(IC_{50})$.[17,18] A 4-fold difference of the IC_{50} values corresponds to a binding energy difference of approximately 1 kcal/mol. As such, the binding energy of $C34_{S138A}$ for the gp41 N-HR was approximately 1 kcal/mol more favorable than that of the binding of C34 to N-HR. Such a small energy difference should play a critical role in increasing/decreasing the anti-HIV-1 activity. Hence, we performed comparative X-ray crystallographic studies on the drug/receptor model complexes of N36/C34 and N36/$C34_{S138A}$ in an effort to understand this energy difference.

Crystallographic study of the six-helix bundle structure with the S138A substitution

The crystal structure of the N36/$C34_{S138A}$ complex is shown in Fig. 2. The crystallographic data are summarized in Table 2. The crystal was indexed to space group *P*321 with unit cell dimensions of $a = b = 49.09$ Å, $c = 56.40$ Å, $\alpha = \beta = 90°$, and $\gamma = 120°$. The structure of the N36/$C34_{S138A}$ complex is a six-helix bundle and is similar to the previously

Table 1. Anti-HIV-1 activities of C-HR-derived peptides against HIV-1 NL4-3(GIV) and thermal stabilities of the six-helix bundles

	EC_{50} (nM)[a]	T_m (°C)[b]
C34	7.3±2.5	67.6
$C34_{S138A}$	2.0±0.4	73.2

[a] EC_{50} was determined as the concentration that blocked HIV-1 replication by 50% in MAGI assay.

[b] Thermal melting temperatures of 10 μM N36/$C34_{S138X}$ complexes (X = S or A).

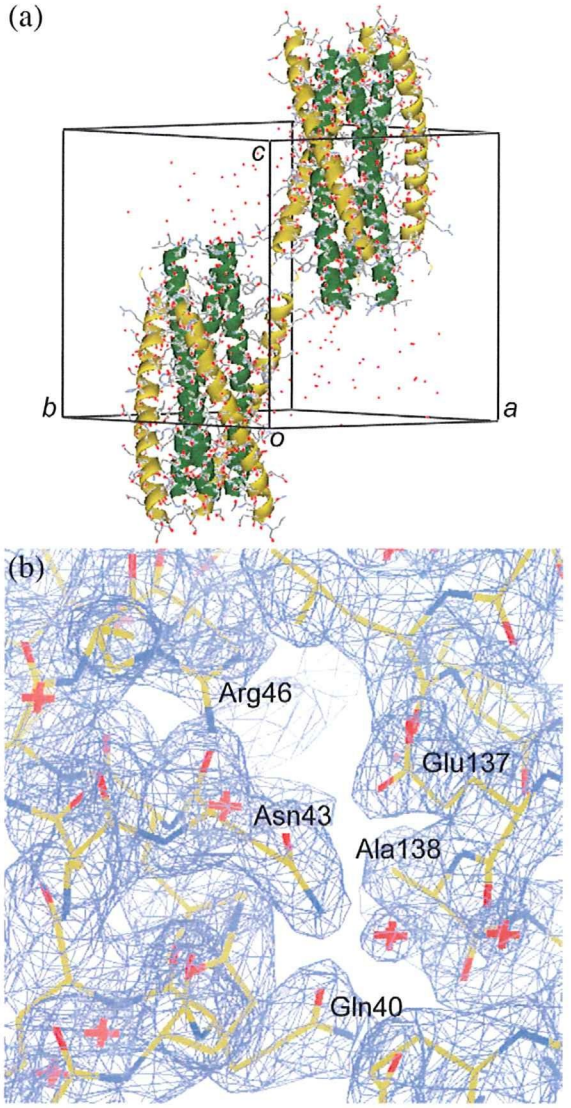

Fig. 2. (a) Crystal structure of the N36/C34$_{S138A}$ complex. N36 and C34$_{S138A}$ helices are colored green and yellow, respectively. (b) Experimental electron density map of the N36/C34$_{S138A}$ complex. The map is contoured at the 1.0 σ level.

Table 2. Crystallographic data for the N36/C34$_{S138A}$ complex (PDB code: 2ZZO)

Space group	*P*321
Cell parameters	
a, *b*, *c* (Å)	49.09, 49.09, 56.40
α, β, γ (°)	90, 90, 120
Data collection	
Resolution range (Å)	33.95–2.20 (2.28–2.20)
Total number of reflections	43,015
Number of unique reflections	4248
Completeness (%)	99.8 (100.0)
Redundancy	10.13 (9.63)
$I/\sigma(I)$	19.1 (4.3)
R_{merge} (%)	6.1 (40.6)
Wavelength (Å)	1.5418
Model and refinement statistics	
Resolution range (Å)	18.52–2.20
Number of used reflections	4037
Number of atoms (non-H)	
Protein	593
Water	27
Mean *B* value (Å^2)	40.7
RMSD bond lengths (Å)	0.026
RMSD bond angles (°)	2.060
R-factor (%)[a]	21.2
R_{free} (%)[b]	28.3
Ramachandran plot (%)	
Most favored	100.0
Allowed	0.0
Generously allowed	0.0
Disallowed	0.0

[a] *R*-factor is a formula for estimating errors in the data set. $R\text{-factor} = \sum | F_{obs} - F_{calc} | / \sum | F_{obs} |$; F_{obs} and F_{calc} are the observed and calculated structure-factor amplitudes, respectively.
[b] R_{free} is calculated using an unrefined subset of reflection data.

reported N36/C34 complex (the C_α RMSD of the two structures is 0.43 Å). The center of this bundle consists of a parallel coiled-coil trimer of the N36 peptides. Three C34$_{S138A}$ peptides wrap in an antiparallel fashion around the outside of the central coiled coil of the N36 peptides. In addition, similar to the N36/C34 complex, the side chain of residue Ala138 packs into the hydrophobic groove and is surrounded by Leu44 and Leu45 of the N36 peptides. Moreover, as shown in Fig. 3, other side chains (Gln40, Asn43, Leu44, Leu45, Glu137, and Gln139) located around residue 138 are near identical in conformation to the N36/C34 complex (the side-chain atom RMSD of the two structures: Gln40, 0.35 Å; Asn43, 0.60 Å; Leu44, 0.34 Å; Leu45, 0.42 Å; Glu137, 0.37 Å; Gln139, 0.85 Å). On the other hand, Arg46 has 1.30 Å side-chain atom RMSD, and

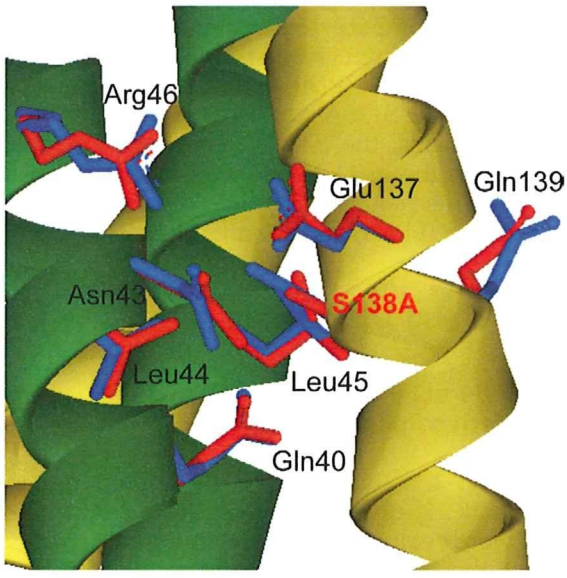

Fig. 3. Superposition of the crystal structure of the N36/C34 complex (PDB code: 1AIK) with that of the N36/C34$_{S138A}$ complex. N36 and C34$_{S138X}$ (X=S or A) helices are colored green and yellow, respectively. In addition, the stick-model side chains (Gln40, Asn43, Leu44, Leu45, Arg46, Glu137, Ser138/Ala138, and Gln139) of N36/C34 and N36/C34$_{S138A}$ are colored blue and red, respectively.

its salt bridge with Glu137 is weakened or broken by the S138A substitution (the distance between the guanidinium group of Arg46 and the carboxyl group of Glu137 is widened from 3.6 to 4.2 Å). These observations indicate that the difference involving the interactions of Ser138 and Ala138 in the C-HR with the hydrophobic groove of N-HR as well as the resulting weakened interaction between Arg46 and Glu137 may influence the N-HR/C-HR complex stability, which relates to the anti-HIV-1 activity.

Currently, based on the X-ray crystal structure of the N36/C34 complex (PDB code: 1AIK), it has been proposed that the S138A substitution increases hydrophobicity and, thus, contributes to a more stable interaction between Ala138 (C-HR) and Leu45 (N-HR) through hydrophobic contacts.[12] In order to confirm the above hypothesis, the binding energies of C34 and $C34_{S138A}$ for the formation of the six-helix bundle were calculated using the X-ray coordinates.

Theoretical calculation of the binding free energies of C-HR-derived peptides

The single-point energy calculations with the FF99 force field were carried out to estimate the effects of the S138A substitution on the formation of the N-HR/C-HR six-helix bundle complex.

Figure 4a shows the intermolecular van der Waals interactions (ΔG_{vdW}) of each residue of C34 and $C34_{S138A}$ monomers in the complexes, which consist of the six-helix bundles formed with N36. The N-HR/C-HR interfacial residues (mainly *a* and *d* positions of the C-HR) of C34 and $C34_{S138A}$ interact strongly within the six-helix bundles. Besides the residues located at the N-HR/C-HR binding

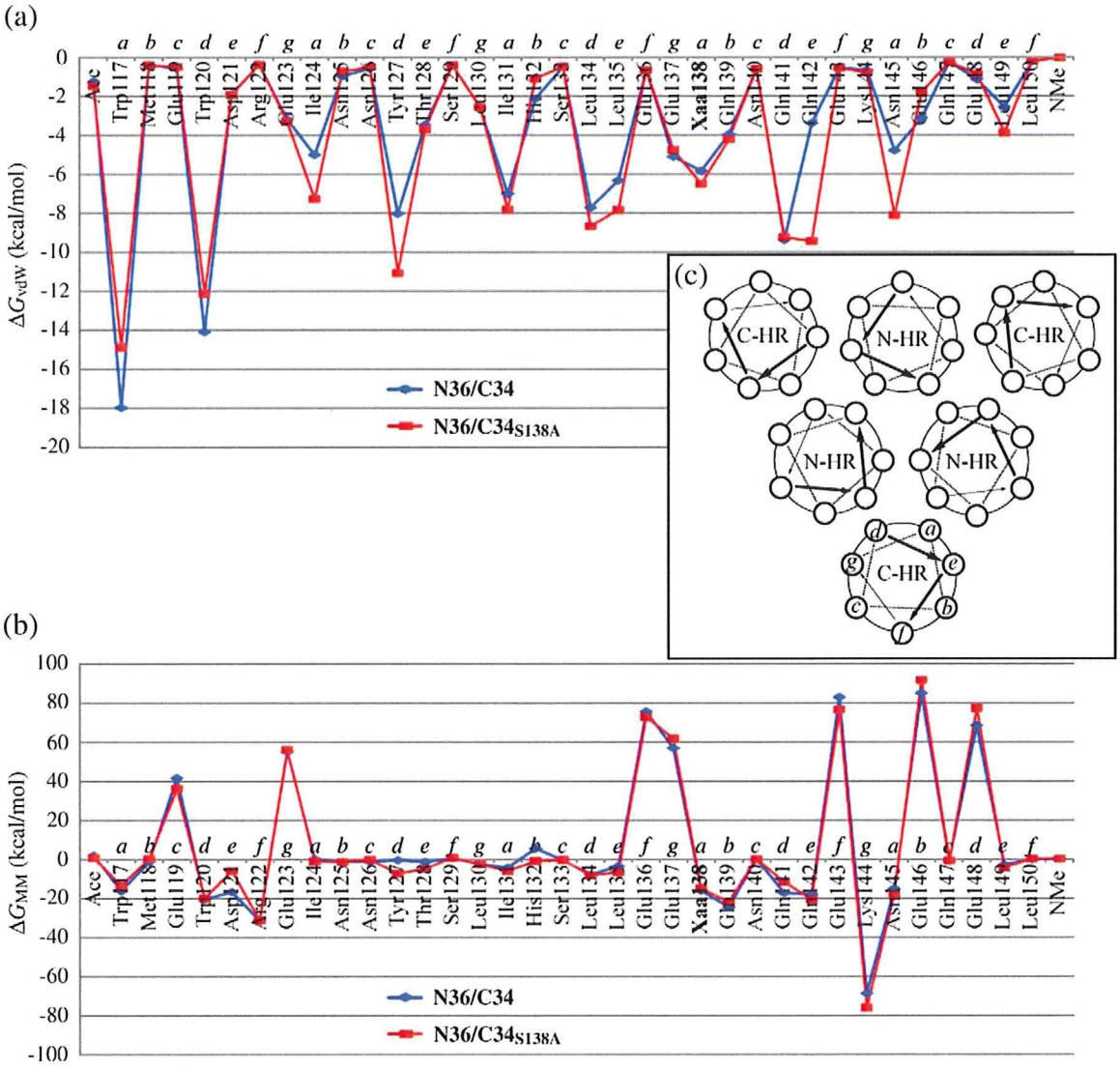

Fig. 4. Intermolecular interactions of each residue of the C-HR-derived peptides in the six-helix bundles: (a) the van der Waals interaction term (ΔG_{vdW}); (b) the pair interaction term (ΔG_{MM}), which combines the van der Waals and electrostatic interactions ($\Delta G_{vdW} + \Delta G_{ele}$); (c) helical-wheel representation of N-HR/C-HR six-helix bundle. The assignments of the residues are presented above the amino acid sequence by the italicized letters. Blue and red lines designate the interactions of C34 and $C34_{S138A}$, respectively.

interface, no significant differences between the ΔG_{vdW} values of each residue of C34 and $C34_{S138A}$ peptides were observed. ΔG_{vdW} of Gln142 located at the *e* position of the C-HR (near the substituted *a* position) was strongly enhanced by the S138A substitution. As shown in Table 3, the ΔG_{vdW} value of the $C34_{S138A}$ monomer was stabilized by 12 kcal/mol relative to the C34 monomer in the six-helix bundle (C34, $\Delta G_{vdW} = -126.76$ kcal/mol; $C34_{S138A}$, $\Delta G_{vdW} = -138.96$ kcal/mol). This indicated that the S138A substitution led to an improvement of the steric interactions between the N- and C-HRs.

Figure 4b shows the intermolecular pair interactions (ΔG_{MM}) of each residue of the C34 and $C34_{S138A}$ monomers in the six-helix bundles. Here, ΔG_{MM} was defined as a sum of the intermolecular van der Waals and electrostatic interactions $\Delta G_{vdW} + \Delta G_{ele}$) serving to stabilize the six-helix bundle structures. The ΔG_{MM} values of all Glu residues (Glu119, Glu123, Glu136, Glu137, Glu143, Glu146, and Glu148) of C34 and $C34_{S138A}$ were estimated as large repulsive contributions. Accordingly, as shown in Table 3, the ΔG_{MM} of C34 and $C34_{S138A}$ monomers in the six-helix bundle structures gave rise to repulsive values (C34, $\Delta G_{MM} = 204.36$ kcal/mol; $C34_{S138A}$, $\Delta G_{MM} = 198.98$ kcal/mol). The repulsive ΔG_{MM} values arise because of the charge–charge repulsion between $C34_{S138X}$ (X=S or A) monomers and the $N36/C34_{S138X}$ (X=S or A) pentamers in the six-helix bundles [N36, +2 charge; C34 and $C34_{S138A}$, −6 charge; N36/C34 and $N36/C34_{S138A}$ pentamers, −6 charge (under standard ionization conditions)]. The Glu119, Glu136, and Glu143 residues (*c* and *f* positions of the C-HR) with small ΔG_{vdW} values were located at the solvent-accessible sites of the six-helix bundles and presumably interact with other species such as solvents or counterions to stabilize the six-helix bundle structures. To account for solvent effects, we applied MM and PBSA[20] methods to calculate the binding free energies (ΔG_{bind}) of C34 and $C34_{S138A}$ (Table 3). Here, ΔG_{bind} was defined as a sum of the intermolecular pair interactions and the desolvation free energies ($\Delta G_{MM} + \Delta G_{solv}$), serving to form the six-helix bundle complexes. The ΔG_{bind} values of C34 and $C34_{S138A}$ were −52.28 and −76.97 kcal/mol, respectively, and showed that both N36/C34 and $N36/C34_{S138A}$ complexes were stable despite the repulsive ΔG_{MM} values. Additionally, the G_{bind} of $C34_{S138A}$ was enhanced by 25 kcal/mol relative to that of C34. The ΔG_{bind} difference arises mainly from the desolvation free energy (ΔG_{solv}) of the $C34_{S138A}$ peptide being larger than the same energy for the C34 peptide (C34, $\Delta G_{solv} = -256.64$ kcal/mol; $C34_{S138A}$, $\Delta G_{solv} = -275.95$ kcal/mol). It seems that the ΔG_{solv} difference directly depends on the hydrophobicity of the substituted residue 138.

Table 3. Results of free-energy calculation by MM and PBSA

Peptides	ΔG_{MM}	ΔG_{vdW}	ΔG_{ele}	ΔG_{solv}	ΔG_{bind}
C34	204.36	−126.76	331.12	−256.64	−52.28
$C34_{S138A}$	198.98	−138.96	337.94	−275.95	−76.97
$C34_{S138A}$ simulation	209.56	−124.99	334.55	−264.94	−55.38

All energy values are given in kilocalories per mole. Peptides were capped with standard Ac and *N*-methylamide groups.

According to the crystal structure comparison between the wild-type and S138A mutant, the structural changes were extremely minor. Thus, we confirmed whether the effects of S138A substitution were predictable by simulation from the wild-type structure after removing the Ser138 oxygen atom. In both the X-ray and simulated structures of the S138A mutant, ΔG_{bind} was enhanced due to the increase in ΔG_{solv}. However, the simulated ΔG_{MM} and ΔG_{vdW} were weakened in contrast with those calculated from the X-ray structure, which was attributable to the different coordinates between the X-ray and simulated structures. This leads to different conclusions about the energy contributions of the S138A substitution and suggests that it is difficult to accurately estimate the mutation effects by simulation from the wild-type X-ray structure.

In order to consider the calculation errors, we performed the free-energy calculations against the candidate structures relaxed by using MM minimization with heavy atoms' positional constraints (Supplementary Data). When the heavy atoms were restrained with force constant 1000 kcal/(mol·Å^2), both the wild-type and S138A mutant structures were optimized with the all-heavy-atom RMSD of 0.01 Å, and these free-energy calculation errors were approximately 1 kcal/mol. Decreasing the force constant by 60 kcal/(mol·Å^2), both structures were optimized with the all-heavy-atom RMSD of 0.05 Å, and the calculation errors with respect to their ΔG_{MM} values were approximately 10 kcal/mol. Thus, the ΔG_{MM} values, which strongly depend on the atomic coordinates, may be inappropriate to understand the energy contributions to the stabilization of the six-helix bundles. On the other hand, the ΔG_{solv} values provided consistent and reliable results for the S138A substitution effects. As such, we concluded that the S138A substitution enhanced the ΔG_{bind} of the C-HR-derived peptide due to the increase in ΔG_{solv}.

We further investigated the ΔG_{vdW} and ΔG_{MM} of residue 138 in the six-helix bundles (Supplementary Data). As shown in Fig. 5, the S138A substitution increased ΔG_{MM} (ΔG_{vdW}) with Leu45. As such, the crystal-structure-based hypothesis that the S138A substitution led to a stable interaction between Ala138 (C-HR) and Leu45 (N-HR) was verified. Interestingly, the difference between the ΔG_{MM} of Ser138 and Ala138 with Leu45 was 2 kcal/mol and would have very little influence on the anti-HIV-1 activity of the C-HR-derived peptide because of the significantly larger ΔG_{solv} difference (25 kcal/mol).

These differences may also be positively involved in viral fusion. Since replication kinetics of variants that have mutations in the N-HR are generally impaired,[24] secondary mutations for efficiently